Launch Lugs Ltd.

Launch Latch

EMA 469: Senior Design
Engineering Mechanics and Aerospace
Department of Mechanical Engineering
University of Wisconsin – Madison

Authors
Kyle Adler
Isaac Becker
Vincent Bensch
Eugene O'Brien
Bryce Quinton

Supervisors
Sonny Nimityongskul
Travis Sheperd
Jon Brooks

December 10, 2024

WISCONSIN
UNIVERSITY OF WISCONSIN–MADISON

Launch Latch

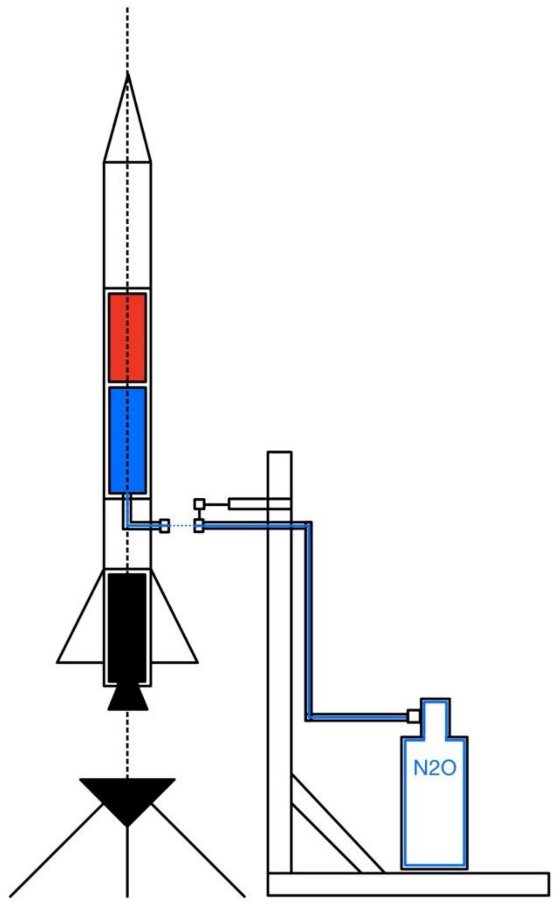

1 Executive Summary

The Wisconsin Space Program (WiSP), a student-led initiative at the University of Wisconsin–Madison, aims to advance amateur rocketry and provide hands-on aerospace engineering experience. As part of its mission, WiSP is developing a liquid-fueled rocket using isopropyl alcohol ($CH_3CHOHCH_3$) as a fuel and nitrous oxide (N_2O) as an oxidizer. The design emphasizes efficiency and safety, particularly in the critical fueling and disconnect processes, to enable safe operation under demanding conditions.

Nitrous oxide, managed above its saturation pressure of approximately 750 *psi* to optimize density and utilize its self-pressurizing ability, presents unique challenges in fueling. Unlike isopropanol, which can be loaded manually, nitrous oxide requires remote handling due to the highly pressurized nature of the oxidizer tank and safety concerns. Additionally, the oxidizer must be supplied just before launch to minimize vaporization and venting losses. These requirements necessitate a propellant quick-disconnect system capable of safely and reliably decoupling the fueling apparatus from the rocket during the launch sequence.

To address these challenges, Launch Lugs Ltd has developed a robust, portable quick-disconnect system with three primary components: a support structure, an actuation mechanism, and a fluid disconnection valve. Together, these components meet critical performance goals and safety standards while maintaining adaptability and cost efficiency:

1. **Support Structure**: Designed for stability and precise alignment, the support structure is adjustable for various rocket sizes, launch configurations, and propellant systems. Constructed from steel for its high strength, durability, and affordability, the structure is lightweight and portable enough to allow for transport to remote launch sites.
2. **Actuation Mechanism**: A spring-loaded linear bearing system retracts the fueling valve and electronics to protect them from rocket exhaust heat during launch. This mechanism ensures rapid and reliable disconnection, minimizing propellant boil-off and mechanical failure risks.
3. **Fluid Disconnection Valve**: Featuring an actuated bayonet connector with a motorized twist-lock mechanism, the valve is engineered for high-pressure applications. For prototyping, the team utilized an off-the-shelf ball-latching disconnect valve actuated by a linear solenoid, balancing cost and reliability.

The system's performance goals include filling 122 *fl. oz*. of liquid oxidizer within 60 seconds and enabling remote propellant tank drainage in the event of a launch abort. It is designed to operate in challenging environments, including extreme temperatures, wind, and dust, with a total system weight under 200 *lbs*. Material selection prioritizes UV stability, corrosion resistance, and durability to ensure a lifespan of at least 50 launches. Comprehensive testing, including pressure, leak, and functionality tests, underpins the system's reliability and safety.

The Launch Latch system sets a new standard for collegiate liquid rocketry by combining technical innovation with practical implementation. By offering a remotely operable, highly adaptable fueling solution, it mitigates risks associated with pressurized propellants, reduces environmental impact through controlled detanking, and enhances the overall safety of rocket launches. This system supports WiSP's broader mission to innovate in amateur rocketry and equip students with skills and experience to excel in aerospace engineering.

2 Table of Contents

3 Introduction

Wisconsin Space Program (WiSP) is both an engineering student organization at the University of Wisconsin – Madison (UW–Madison), and the UW–Madison chapter of the American Institute of Aeronautics and Astronautics (AIAA). WiSP aims to both interest students in, and prepare them for, careers in Aerospace Engineering. According to the Bureau of Labor Statistics, there were 68,900 Aerospace Engineering positions in 2023, projected to grow by 6% over the next decade [1]. Building and launching rockets as part of WiSP gives students valuable practical experience in their field of choice, exposure to concepts that are only covered late in the course of an Aerospace Engineering degree, if at all, and practice working in teams, a skill universally required of Engineers in industry.

Solid rockets of various power levels are the backbone of collegiate rocketry teams nationwide. There is a significant ecosystem built around their construction and safe operation. The National Association of Rocketry (NAR) and Tripoli Rocket Association (TRA) each offer certification levels for high-powered rocketry targeted at standardized classes of solid rocket motors. These rocket motors, and kits to construct them, are commercially available. While a somewhat niche market, multiple suppliers exist for parachutes, ignitors, launch rails, telemetry systems, and aerodynamic shells. This ecosystem allows new teams to gain experience with pre-built rockets before designing their own. More experienced teams can focus on the design and construction of specific elements, while procuring others ready to use. Even fully self-designed high-powered solid rockets are well within reach for collegiate teams, with potassium nitrate (KNO_3) and sugar being a popular starting point for solid fuel chemistry.

In real-world applications, liquid fueled rockets are the norm. In 2023 there were 219 rocket launches intended to reach earth orbit[1]. The most common launch vehicles were the Falcon-9, Long March family[2], Electron, and R-17. Together they accounted for 75% of orbital launches, and are all liquid fueled [2]. While they are consequently valuable for student teams to explore, they require pressure vessels, valves, a combustion chamber or catalyst bed, an injection system, and other elements not present in solid rockets, making their design, construction, and operation significantly more complex. Further, liquid fueled rockets lack the kind of standardized or commercially available solutions available for solid rockets, which presents teams with a steeper learning curve. The difficulty of designing these systems presents opportunities for students to grow their engineering skills and build greater familiarity with rocket systems they hope to work with in a professional capacity.

[1] This figure includes failed launches

[2] Excluding the single Long March 11 launch, which is a solid fueled rocket

3.1 Problem Statement

WiSP is developing liquid fueled rockets. The rockets currently in development require the oxidizer tank to be a pressure vessel. The oxidizer tank has a limited safety factor due to the mass limitations inherent to rocketry. Were the tank to rupture, people near the rocket could be injured by shrapnel. Therefore, the oxidizer must be loaded after all personnel have retreated to a safe distance. Currently the clip holding the oxidizer line to the rocket is secured to the ground, and the launch of the rocket pulls the clip off, allowing the oxidizer line to fall free. This can be seen in Figure 3.1.1. If the clip failed to separate, the oxidizer line and rocket could be damaged, the launch could fail, and the rocket could even be directed off course, becoming a hazard. Additionally, the only way to abort launch with the clip design involves dumping nitrous out of the nozzle, which has environmental and safety concerns, as well as wasting the oxidizer. These hazards can be mitigated by designing a fueling system that can be remotely ordered to disconnect from the rocket, report a successful disconnection before launch is initiated, and can rapidly dump the oxidizer into a tank for later use.

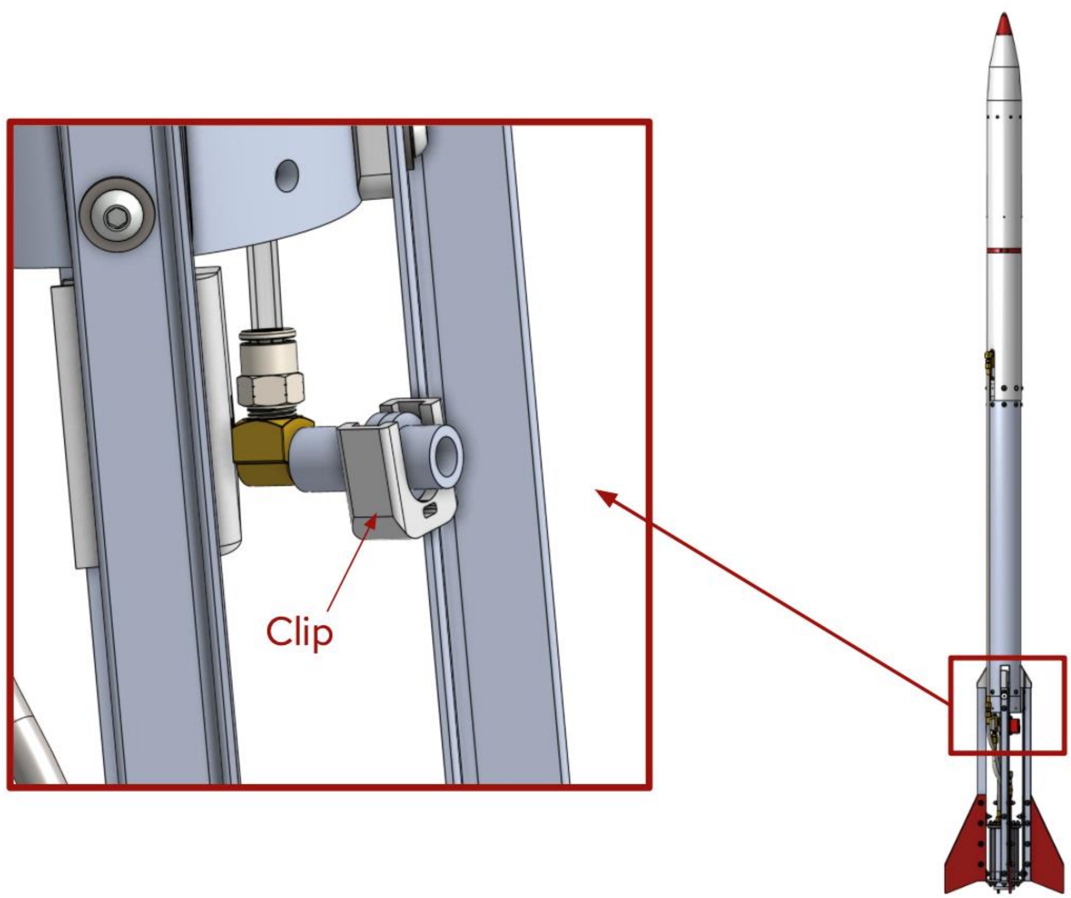

Figure 3.1.1. Liquid rocket (right) and clip connector design (left)

4 Applicable Designs

In the development of the Launch Latch, the project team is exploring both competition and patents to identify proven designs, technologies and mechanisms that can inform and enhance the project. Analyzing solutions from the aerospace industry and rocketry hobbyist, can provide an understanding of the challenges and opportunities related to propellant transfer and quick disconnect systems. Patents are also important to review to ensure that the Launch Latch design avoids potential design pitfalls while also not infringing on any intellectual property.

4.1 Competition

The Wisconsin Space Program's Launch Latch for amateur rocketry draws inspiration from multiple aerospace industry sources, including the Northrop Grumman Mission Extension Vehicle, orbital launch towers, as well as the designs employed by rocketry hobbyists and clubs. While the project does not strictly adhere to the specifications of these systems, past innovations provide valuable insights into mechanisms needed for successful propellant transfer and disconnection.

The Northrop Grumman Mission Extension Vehicle (MEV), although focused on in-space satellite servicing, offers key lessons in system robustness and remote operational capabilities. The MEV's successful docking with geosynchronous satellites demonstrates the precision and reliability required in space-based systems, see Figure 4.1.1. Some of the most applicable features to the Launch Latch is the MEV's ability to service multiple satellites within its lifetime due to its compatibility with nearly 80% of all GEO satellites. The MEV is capable of this due to is high mobility of its robotic arm. The Launch Latch will be translating this design criteria to have a high level of adjustability to be compatible with many different rocket propellants, launch rails, and rocket geometries [3].

Figure 4.1.1. Northrop Grumman's MEV (left) servicing a target satellite (right) [2].

Towers for orbital launch vehicles like NASA's Space Launch System (SLS), SpaceX's Starship, and Blue Origin's New Glenn provide direct analogs in handling large volumes of propellants under demanding conditions and more applicably, methods of arm retraction. NASA's SLS and SpaceX's Starship uses sophisticated launch tower systems, as seen in Figure 4.1.2 and Figure 4.1.3, respectively, that employ many different arm retraction variations including rotating arms either parallel or perpendicular to the vertical axis of the rocket. This detachment process is coupled with either a linear disconnection or umbilical tear away. Due to lesser concerns from exhaust heat, Launch Latch will employ only the linear motion disconnect to allow for higher reliability on the disconnect mechanism [4] [5] [6].

Figure 4.1.2. NASA's SLS quick disconnect arm variations [5]

Figure 4.1.3. SpaceX's Mechazilla propellant and power quick disconnect for Starship. [6]

Blue Origin provides a new prospective of retraction method with their rapid retract system for New Glenn. This method includes the entire tower hinged at the base as seen in Figure 4.1.4. Regarding the Launch Latch, this method would require a large about of torque to actuate the full structure and arm, which is undesirable due to it greatly increasing the required battery power requirements. However, this will be considered for a manual adjustment to allow for an additional rotational degree of freedom to align the linear actuation. [4]

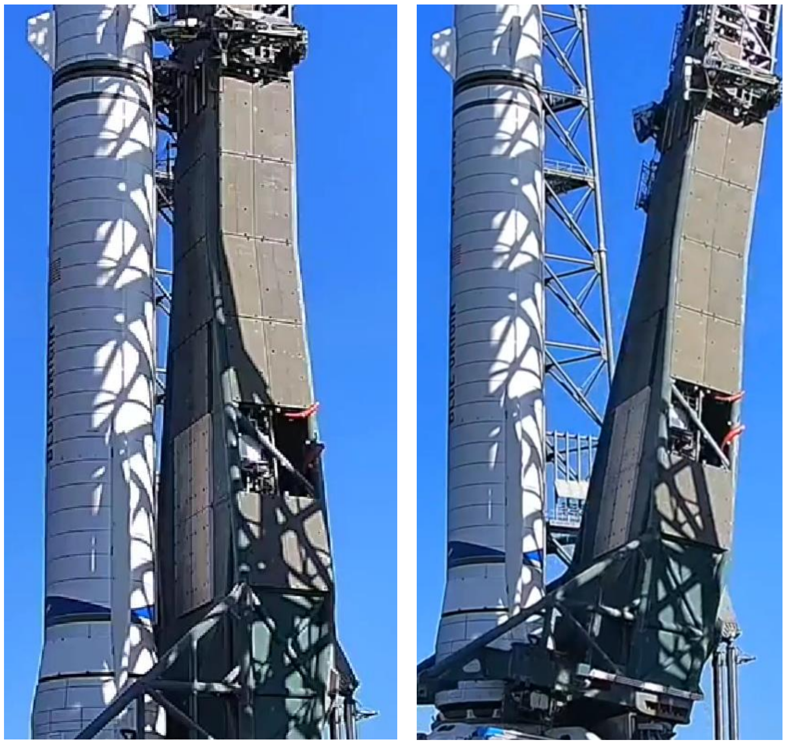

Figure 4.1.4. Blue Origin's rapid retract system for New Glenn. [4]

Another critical aspect of orbital launch towers and the Launch Latch is rapid disconnection under high-pressure conditions, such as those encountered during a launch sequence or in the case of an abort scenario. While the propellant in this project, N_2O, is not stored at cryogenic temperatures, the handling procedures used for cryogenic fuels in HLLVs offer important lessons for dealing with volatile substances like N_2O [4] [5] [6].

The Launch Latch aims to incorporate a detanking capability to safely recover the oxidizer in the event of an abort, orbital launch towers do so through the use of pumps and pressurized gases to fill and drain propellants. In amateur rocketry, such mechanisms are rare, with teams often relying on manual venting. Launch Lugs Ltd. seeks to pioneer a more efficient solution by achieving controlled detanking without the need for additional gas storage or pumps, setting a new standard for safety and functionality in amateur rocketry.

Beyond large-scale industry applications, rocket hobbyists and rocketry clubs offer practical, creative approaches to quick disconnect systems, particularly for smaller, cost-effective builds. Many hobbyist designs emphasize lightweight, adaptable materials that prioritize portability and modularity—features central to the quick disconnect tower design. The modular systems used in amateur rocketry often employ quick disconnect mechanisms designed for rapid assembly and disassembly, ensuring ease of transportation and operational flexibility. These designs typically prioritize fuel line safety and pressure stabilization, providing valuable insights for achieving high performance on a limited budget. As seen in Figure 4.1.5 and Figure 4.1.6, two examples of hobbyist designs, both groups opted for the linear motion for the increased stack-up reliability discussed in the previous section [7] [8].

Figure 4.1.5. Linear actuated quick disconnect build by Exciting Crapo for hybrid rockets [8]

Figure 4.1.6. Oregon State University AIAA Club's cryo quick disconnect for their High-Altitude Liquid Engine (HALE) [7]

The Launch Latch benefits from the diverse innovations and lessons drawn from industry leaders like the MEV and orbital launch towers, as well as the creative solutions developed by rocketry hobbyists. These sources provide the foundation for developing a reliable, safe, and modular quick disconnect system capable of handling the wide range of launch criteria as specified in the product design specification.

Away from rocketry, many other forms of remote fueling quick disconnects exist. One of which being air to air refueling where one jet transfers fuel to another through a probe and drogue as seen in Figure 4.1.7. Although the Launch Latch will not have the requirement of remote connection, many other aspects of the process can be applicable to the launch latch. Some of these include feedback solutions to understand the state of connection and propellant from a distance to execute launch based on the feedback [9].

Figure 4.1.7. Royal Air Force Typhoon FGR4 performing in-flight refueling from through a probe and drogue [9].

4.2 Patents

Several patents exist for the quick disconnect mechanism, detailing critical aspects necessary for high-pressure propellant transfers. Many of these are patented by NASA, including US3656781A [10], a quick-disconnect coupling suited for umbilical leads, aligning closely with this project's intended usage. While it incorporates capabilities for electrical connections in addition to fluid transfer, its ball-and-groove locking mechanism, as seen at find number 52 in Figure 4.2.1, is particularly relevant for ensuring a secure and quick release, a feature that could be adapted for use in the propellant quick disconnect tower [11].

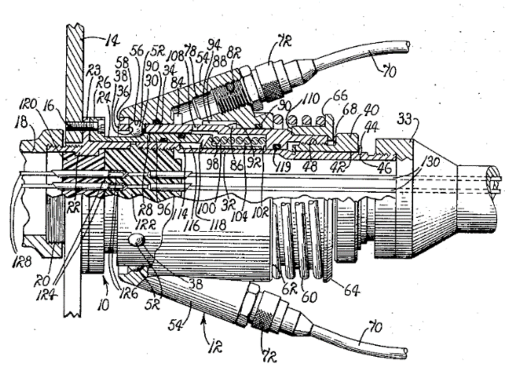

Figure 4.2.1. US3656781A: Quick-Disconnect Coupling with ball-and-groove locking mechanism [11].

A patent, US5116021A [12], from Deka Products LP, presents a different perspective as seen in Figure 4.2.2 by using a disk seal, find number 42, that closes upon disconnect and a pin mechanism that opens flow once connected. This design offers valuable insights into preventing leaks during disconnection, although its lack of a dedicated locking feature and potential for side load issues could pose challenges for the scope of the Launch Latch [12].

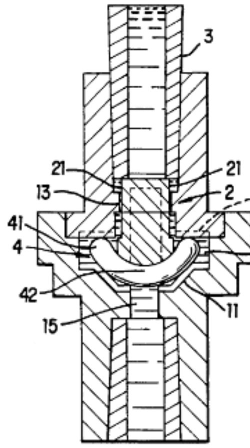

Figure 4.2.2. US5116021A: Quick-disconnect valve with elastic disk for sealing [12].

Finally, US10730646B1 [13], another NASA patent, specifically addresses oxidizer nozzle tools and quick disconnect systems, making it highly applicable to this project. The patent combines linear actuation for retraction and rotary actuation for engagement. Its rotary drive mechanism, find number 208 in Figure 4.2.3, for low-force connection and disconnection could provide useful design inspiration due to our criteria to not impose a side load on the rocket prior to launch, although its complexity might exceed the project's needs. Nonetheless, this patent highlights advanced mechanical methods for linear actuated disconnects [13].

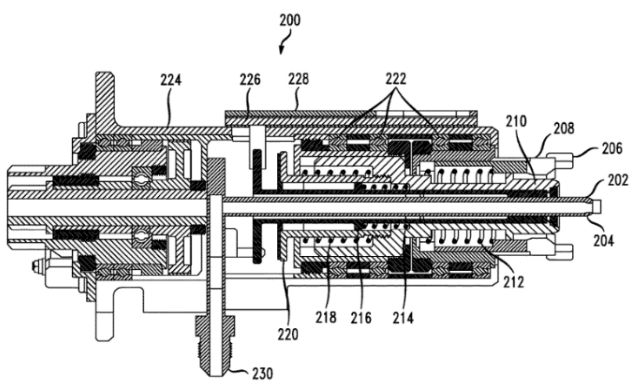

Figure 4.2.3. US10730646B1: Oxidizer nozzle tool and low separation force quick disconnect system for fueling [13].

5 Design Specifications and Criteria

In order to characterize the design, evaluate performance and compare prototype designs, there are a number of different criteria that guide development and criteria that must be met by the corresponding component. The full list of design specifications can be found in Appendix A: Preliminary Design Specifications (PDS), and the critical design specifications are as follows: The device must be adjustable to various lengths and diameters of rockets, locations of fill valves, and various types and sizes of launch rails. It must be fully remotely operable and safe prior to physical operation before and after launch. All tubing and flow control devices shall safely withstand the pressures and chemical properties of saturated nitrous oxide at desired flow rates throughout the temperature range of 0°F to 120°F. It may be manually attached but must remotely detach from the corresponding inlet on the rocket. It also must provide a means to evacuate the pressurized propellant from the rocket tank in the case of a launch abort. Lastly, the device must be compatible with existing propellant tanks and lines as desired.

5.1 Performance

Performance is the most important criteria, as the functionality will dictate the success of the project. At the saturation pressure of temperatures within the given range (roughly 300-1100 psi), the design must be able to fill at least 122 fl. oz. of liquid oxidizer (around 6 lbs of N_2O) in around 60 s, for a flow rate of around 2 fl. oz./s [14]. It must perform the filling operation fully remotely and disconnect when it receives signal from the rocket flight computer. It must be able to drain the rocket propellant tank remotely in case of aborted launch. Any leaks in the fluid system should be minimal and restricted to temporary operations (disconnecting valve, venting tank, etc.).

5.2 Environmental

The project should function and be recoverable in a desert environment, including factors such as heat, dust, wind, and direct sunlight. Similarly, it must withstand heat from exhaust and debris kicked up by takeoff. The design must function in an ambient temperature range of 0°F to 120°F, pressure range of 13 to 17 psi, humidity ranges from 5% to 95%, sand at 20 mph, resting on snow if tested during winter months, and any electronics enclosures must be rated to IP5X [15] to provide reasonable resistance to ingress of dust.

5.3 Size and Weight

The final design needs to be portable in order to be transported to different launch sites, and needs to fit in a car trunk (roughly the size of Chrysler Pacifica or similar minivan, 4 ft by 8 ft). The height must be adjustable and tall enough to reach the fueling point and match the angle of the valve on the rocket (2 ft to 6 ft, valve angled up to 15° from horizontal). It should be light enough to be carried by two reasonably fit people for a quarter mile, since the rail may not be directly accessible by vehicle. Multi-part assembly on site is acceptable, but should weigh no more than 50 lbs per piece if it is in multiple pieces. The entire design shall weigh no more than 200 lbs including any counterweights for stability.

5.4 Materials, Maintenance and Lifespan

The fluid plumbing must be compatible with all foreseen propellants, specifically N_2O. The tower structure material must be able to withstand high heat and support loads from the propellant tank (~30 lbs). The design must use materials that will resist corrosion, warping from temperature, and abrasion from sand, and any plastics must be UV-safe. Regular maintenance should include cleaning and inspection, ensuring that no hazardous chemicals remain on surface and no structural sections are damaged. It must be reusable for at least 50 launches, including static fires, test launches, and competition launches. Some components may be designed to be replaced periodically or before every launch.

5.5 Testing

Several components shall undergo qualification testing before first use, and be tested for functionality before every subsequent use, including the valves, fluid components, and the electromechanical systems that facilitate the disconnection. A risk assessment will be done once parts are well defined. Pressure and leak tests will be conducted using NASA Leak Test Requirements, including the following: Dry test without rocket to ensure electronics function (electromechanical system should function as intended), wet test with low pressure water to ensure plumbing functions (plumbing system should function without leaks), and dry test with rocket to ensure coupling and decoupling (system should disconnect repeatedly without failure) [16].

5.6 Safety and Environmental Impact

The control mechanism for the rocket and ground support system should not allow rocket flight if the disconnect mechanism fails to activate, and should have a dump failsafe in the case of connection loss. Much of the rocket's safety procedures rely on remote operation and standoff distances from pressurized N_2O, thus the project must incorporate those procedures into the operation of the arm before, during, and after launch.

The design must have pressure relief valves and/or burst disks to avoid over pressurization for pressures associated with saturated nitrous oxide. The fluid system must also be safe with any foreseen static electricity, to avoid ignition risk with potent fuels and oxidizers nearby. The design should avoid pinch points on tubing with any moving parts.

The project shall minimize leakage that could impact the environment and aim to prevent additional hazardous gasses from releasing into the atmosphere. Small leakage immediately following disconnect may be unavoidable, but the design must not have any prolonged leaks, and should safely dump propellant into a separate vessel in the case of a launch abort. Venting to the atmosphere should also be avoided where possible since N_2O is a potent greenhouse gas. Structural components should be made of recyclable metals.

5.7 Human Interfacing and Public Impact

The project must be fully remotely operated in conjunction with the main rocket ignition signal. It must be easy to adjust and set up on launchpad by WiSP and other student organizations. This product will neither be marketed at, be made accessible to, or be operated near the public. The design should allow for more student organizations to fill liquid rockets safely which will allow more social classes access to aerospace activities; the aerospace industry is rapidly growing in the United States and this product would allow more student orgs and hobbyist to grow their knowledge.

6 Design Concepts

The project has several distinct facets that need their own criteria and design work, namely the fluid connection point, the actuation device, and the support and alignment structure. All the ideas generated during brainstorming were put into one of these categories and evaluated based on their own sets of criteria.

6.1 Structure and Alignment

The support structure for the fueling mechanism is very important. A solid structure will keep the connection/disconnection mechanism in place despite environmental conditions, ensuring successful repeated fueling and detaching cycles. The structure also governs the alignment ability of the fueling mechanism, allowing it to fit exactly into the rockets fueling stud. All the brainstormed ideas fit either into a one-pole or two-pole design. Figure 6.1.1 is the two-pole design. Figure 6.1.2 is the one pole design. The pole design allows for the joint and actuator system to slide up and down the pole seamlessly. Other sorts of geometry require more intricate clamps to integrate with the other systems. The two pole designs were the only designs considered for the structure since the disconnect system needs to be able to work from the height of two to six feet. The pole design allows for the most accurate and efficient adjustment.

Figure 6.1.1. Two Pole Design CAD Mockup.

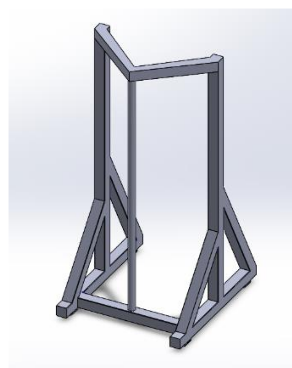

Figure 6.1.2. One Pole Design CAD Mockup.

Each design would have a similar supporting base but would differ in the tower section of the supporting structure. The two-pole design would have two parallel rods that support the fueling mechanism and would use collars with friction-fit screws to adjust the mechanism’s height. The one-pole design would use only a single vertical rod and would support the mechanism using a microphone-stand-style support. Figure 6.1.3 is what the pole clamp would look like for the one pole system.

Figure 6.1.3. Pole Clamp design for the single pole system.

The stability parameter considers the structural rigidity of the support, as well as the amount of weight it could potentially hold. Stability was given a weight of three since the disconnection system only needs to stay up after connected. The cost parameter considers both the monetary and time cost associated with purchasing and fabricating each design. The cost was weighted a three due to the budget induced by the club, but it does not need to be a limiting factor. The weight parameter considers how heavy and easily transportable the design would be, with a higher number being lighter and easier to transport. There will be many ways to deal with the weight and transportation of the system, so the weight was given a weight of one. The degree of freedom parameter considers how adjustable the joint(s) between the support rods and fueling mechanism will be, to ensure alignment with fueling stud. The last and most important criteria is the degrees of freedom, since it will need to be able to attach to the rocket valve from any angle. Therefore, the degree of freedom has a weight of five. The associated pros and cons of each design are summarized in Table 6.1.1.

Table 6.1.1. Design matrix for the structure and alignment designs.

Structure/Alignment	Weight	Concept 1 (Two Pole Structure)	Concept 2 (One Pole Structure)
Stability	3	5	3
Cost	3	3	5
Weight	1	1	3
Degree of Freedom	5	3	5
Weighted Total		34	42

While the two-rod design is more stable, it has a higher cost and would be heavier as well as affording two less degrees of freedom. While it would be easy to alter the inclination of the fueling mechanism, altering the lateral angle would require moving the entire support structure. The one-rod design is slightly less stable, but costs less and is lighter. Additionally, with an optical pole clamp style joint, the inclination and lateral angle of the fueling mechanism can easily be altered without moving the entire structure. Due to these factors, the team will be moving forward with the one-rod structure design.

6.2 Actuation Methods

To refuel and disconnect successively, linear motion will be required to detach the fueling mechanism from the rocket. During our design process, it was determined that reconnection is no longer a priority. The actuator must simply be reliable enough to achieve 1D linear motion quickly.

A pneumatic actuator would be able to leverage the high-pressure gas in the fueling system. By diverting some of the oxidizer to a pneumatic piston, the fueling valve could move back and forth. Several more conventional approaches include a rack and pinion powered by an electric motor, and a commercial off the shelf electronic linear actuator. A simpler approach would be a spring-loaded linear bearing, that would release a stop and be pulled away from the rocket by a spring.

In the Table 6.2.1, the cost parameter considers both the money and time that would need to be spent purchasing and fabricating each design. The ease of control parameter considers the complexity of the electronics behind controlling each design. The stroke length parameter considers how large a stroke length could be easily retained. The speed parameter considers how quickly each actuator can be retracted. Most important are the speed and stroke length, ease of control is of medium importance, and cost is of minimum importance.

Table 6.2.1. Design matrix for the actuation methods to get the valve to and from the rocket.

Actuation Methods	Weight	Concept 1 (Pneumatic)	Concept 2 (Rack and Pinion + Motor)	Concept 3 (Electric Linear Actuator)	Concept 4 (Spring Loaded Linear Bearing)
Cost	1	3	3	1	5
Ease of Control	3	1	5	3	3
Speed	5	5	3	1	5
Stroke Length	5	3	3	1	5
Weighted Total		46	48	20	70

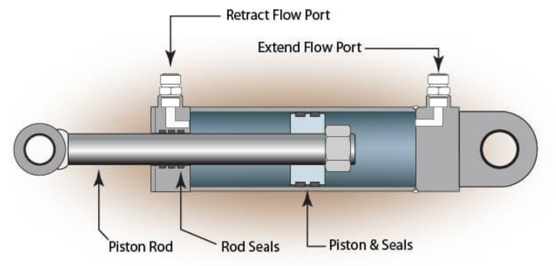

Figure 6.2.1. Pneumatic Actuator [17]

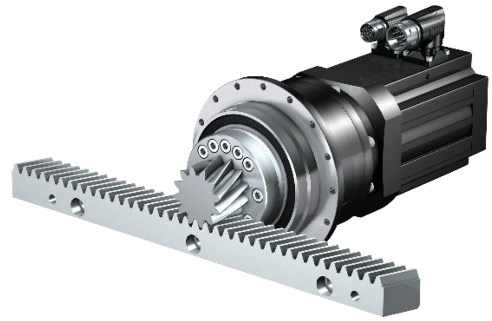

Figure 6.2.2. Rack and Pinion [18]

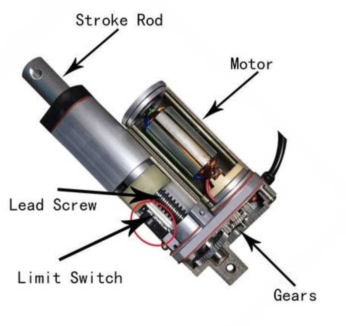

Figure 6.2.3. Electronic Linear Actuator [19]

Figure 6.2.4. Linear Bearing & Spring. Spring attaches to collar.

The pneumatic design would be quick and powerful, but hard to control electronically and less precise than the other options. It would also siphon gas needed for the rocket, or otherwise require an external tank of more pressurized gas. The rack and pinion design is conventional and easy to implement, but ultimately lacks the speed required. While an off the shelf linear actuator would be precise and relatively easy to control, the stroke length required would necessitate an incredibly heavy model and has nowhere near the required speed to clear the rocket fuel plume in time. The spring/linear bearing design is cheap, easy to control, and exceedingly fast. The only control it would require is a pulse signaling the release of the stop, and a servo to achieve that motion. Thus, the spring-loaded design will be used.

6.3 Connect/Disconnect Valves

Finally, the fluid connection/disconnection valve needs to be able to pair the oxidizer lines while not failing at high pressures and be easy to disconnect.

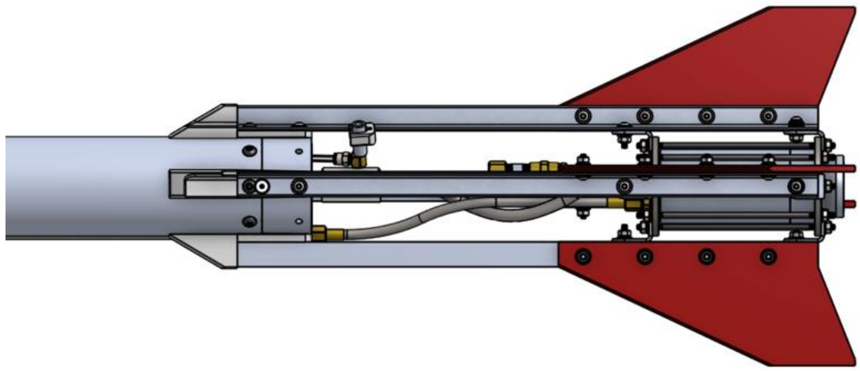

Figure 6.3.1. Aft section of a liquid model rocket, with the existing clip quick disconnect design [14].

An actuated bayonet involves a bayonet connection and an additional securing motor to twist the connection point into a corresponding clip on the rocket. This design is optimized for reconnection. A student Manufactured Quick disconnect could be created to maximize the ease of disconnection. An off-the-shelf disconnection could also be purchased, which would guarantee a high-pressure rating.

The ease of connection and disconnection parameter considers how intricate the mechanism for disconnecting would need to be for each design, with a higher number being the simplest. The pressure rating parameter considers how much pressure valves of each variety can support without failing. The cost parameter considers both the monetary and time cost associated with purchasing and/or fabricating each design. Pressure rating is the most important, ease of disconnection is of middling importance, and cost is the least important.

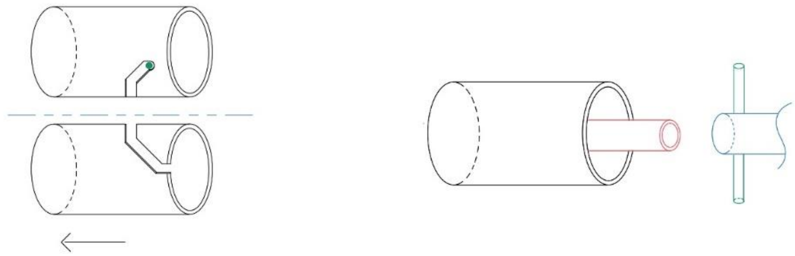

Figure 6.3.2 Left Figure is the path the bayonet extensions follow as the valve is inserted into connection. Right figure is the overall bayonet valve.

Figure 6.3.3. Push-fit fitting [20].

Figure 6.3.4. Ball latching fitting [21].

Table 6.3.1. Design matrix for the disconnect/connect valves for the hose and rocket connection.

Disconnect/ Connect Valves	Weight	Concept 1 (Actuated Bayonet)	Concept 2 (Quick Disconnect + Servo Mechanism)	Concept 3 (Off the shelf Quick Disconnect)
Ease of Disconnection	3	1	5	2
Pressure Rating	5	3	3	5
Cost	1	1	3	3
Weighted Total		19	33	37

The actuated bayonet design was optimized for reconnection, which is no longer a priority. As such, it is hard to disconnect and not necessarily optimized to contain pressure. While a manufactured quick-disconnect could be designed to maximize ease of disconnection, there would not be enough time to extensively test it to ensure that the determined pressure rating is accurate. An off-the-shelf quick disconnect, while slightly harder to engage disconnection, would provide the most reliable pressure rating. As such, the off-the-shelf quick disconnect will be utilized.

7 Standards

Since this project will be used by the Wisconsin Space Program to fuel and refuel the liquid rockets launched by the club, there are standards and rules depending on the competition the student organization is participating in. This disconnect system is not directly related to any competition, but a piece of equipment that will be used across competitions. The standards used for this project will be based on NASA requirements for their liquid propelled rockets. The chosen standards focus on the ground support equipment for the liquid rocket instead of the rocket itself. The ground system standards are chosen because the project focuses on ground equipment that will be able to fuel and refuel the rocket remotely. Additional standards are included in this project that focus on other parts that are not specifically stated in the NASA ground equipment standard.

7.1 NASA Standards

The main standard that will guide the entirety of this project with be Standard for the Design and Fabrication of Ground Support Equipment, NASA-STD-5005D [22]. This set of standards was chosen since the project focuses on the ground support equipment for the liquid rocket. This standard was designed to create basic requirements for equipment that will help prepare the rocket for flight. There are multiple standards referenced within the NASA standard for specific parts of the designs. The main sections of this standard set that will relate to the project are materials, testing, valves, and design [22].

There will be pressurized systems and pressure vessels throughout the design. Within the pressurized system, there will be a high pressurized valve that operates above 1000 psi. There will be pressurized hoses containing fuel. Based on this requirement of the project, the pressurized system design will follow NASA Standard for Ground-Based Pressure Vessels and Pressurized Systems. This set of standards is also known as NASA-STD-8719.17 [10]. The pressure vessels and pressurized systems this project will contain will be on the ground. NASA-STD-8719.17 refers to a specific standard for pressurized vessels [10]. In addition, the ASME specification for Boiler and Pressure vessel code, Section VII is the main standards for the design and fabrication of pressure vessels [10] [23].

7.2 Relevant Standards

The pressurized system will contain two different chemical species. The main chemical species that must be considered will be Nitrous Oxide. It is important to design the project and system so it can withstand Nitrous Oxide. Therefore, AIFA 081/16 will be used to help design the project [24]. This standard focuses on the safe use and storage of nitrous oxide and compatible materials for tubing and pressure vessels [24].

There will be a quick connect and disconnect valve for fueling the rocket integrated and designed within the project. Valves have certain standards that need to be met to allow for use by others. The Standard Specification for Quick Disconnect Couplings will be used to guide the design and fabrication for the valve. The standard is ASTM F1122-22 [25]. This will allow for the valves to be used on multiple different rockets by following industry standards. The valve will be designed specifically for this rocket but also ones that will be launched in the future [25].

The structure that will hold the valve disconnect system will have welds and threaded fasteners to keep the part together. This was done to keep the system modular and easily transportable. The NASA standard for threaded fastening systems in spaceflight hardware will be used for this project. This standard includes the spacecraft, but also all the equipment that is used in tandem with it. The standard is NASA-STD-5020A [26]. The NASA welding standard for aerospace materials, NASA-STD-5006A, will be followed for this disconnection system as well since it is interfacing with the rocket [27].

8 Design Conclusion

To conclude, the project designs have been chosen after a thorough evaluation of the specific design criteria for the project. The project will also consider the previous patents and competition to not infringe on others while following the NASA standards. The support structure moving forward will be a single pole design that will allow for more degrees of freedom. The additional degrees of freedom will allow for ease of connection of the valves. The valve will be the actuated bayonet connection due to the higher-pressure rating and the minimal load on the rocket during attachment and detachment. The activated bayonet will be easier to attach and detach compared to the other options that could withstand the high pressure. Lastly, the electric linear actuator will be used for the simplicity and the accurateness of the method. The three different parts will combine to create a remotely detachable refueling system for liquid rockets.

9 Analysis

The analysis of the Disconnect System was done following the NASA Standards specified in the Standards section and competition guidelines. For each part a different analysis was performed to ensure that it would function properly. The structure, arm, and actuation method are more mechanical analysis. While the value has structural analysis, but also a lot of fluid and thermodynamic analysis.

9.1 Structure Analysis

The analysis of the structure is essential to ensure that the arm and actuation method can perform the desired operation. The main modes of failure for the structure are tipping of the entire system or a member yielding under the forces. The factor of safety for the structure is two based on the NASA Ground Support Equipment standard [22]. The structure consists of four different parts which are the base, feet, support, and the pole. The pole and feet are the main components of concern when it comes to stress since they will be bearing most of the load compared to the support and base. The material for the different parts will be mild steel. The yield strength of the mild steel is *42 ksi* [28]. The different components of the structure can be seen in Figure 9.1.1. The origin is in the back right corner. Each component is located with reference to the origin.

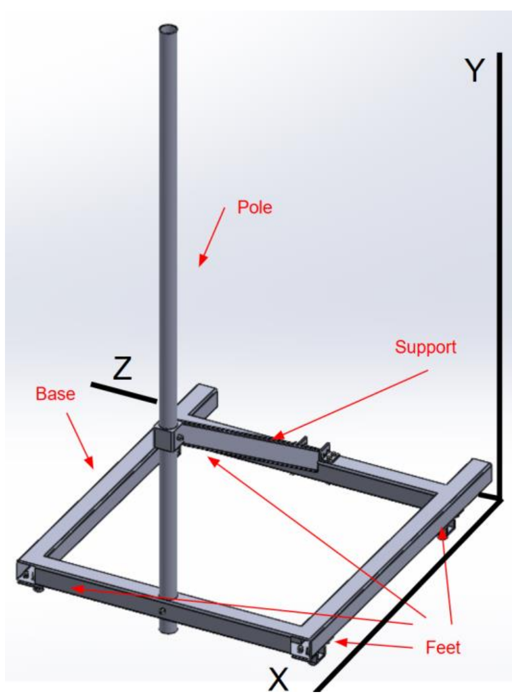

Figure 9.1.1. Different parts of the structure.

9.1.1 Tipping Analysis

Tipping is the main mode of failure that the structure is concerned with since it would fall into the rocket upon disconnect. The weight of the structure was determined based on a square steel stock of 2.5x2.5 *in* with a thickness of 0.120 *in* and a pole with a 2 *in* diameter and a thickness of 0.120 *in*. There is an additional counterweight force that will be considered. In Figure 9.1.2 the counterweight force is denoted at cw. There needs to be a counterweight force on the structure to prevent the entire structure from tipping from the weight of the arm and actuator. For the tipping analysis, the whole system was analyzed as a rigid body. First, the center of mass was found of the entire system to simply calculate the moment due to the mass. The equation for the center of mass of the x component is

$$x_{com} = \frac{\sum x_i m_i}{\sum m_i} \tag{9.1.1}$$

where x_i is the x position of the center of mass of one part and m_i is the mass of the respective part. This can be done for each coordinate as well.

Once the center of mass was found, the force due to the wind was calculated. This can be found using the dynamic pressure equation multiplied by a drag coefficient and respective area. The equation is

$$P = \frac{1}{2}\rho V^2 C_D A \qquad (9.1.2)\ [29]$$

where ρ is the density of air, V is the worst-case velocity, which is roughly 30 mph in the desert, C_D is a drag coefficient based on geometry, and A is the area that is affected by the dynamic pressure. The 30 mph gusts of wind were determined from experience in other launches in the desert. The rocket will not launch in this condition; however, the stand will not be able to be moved under these conditions. The drag coefficient for circular pipe and a rectangle were chosen for this analysis. The circular drag coefficient is used for the pipe which has a value of 1.2, and the rectangular drag coefficient of 2 is for the bar stock [29]. The P force will act at different locations depending on the direction of the wind, but the worst-case scenario will be looked at.

The other forces that act on the structure are defined by its mass in addition to the arm and actuator. The F1 and F2 forces are resultant forces from the mass of the arm and actuator and disconnection force of the valves. These are acting at the top of the pole to simulate the largest moment that could be induced by them. The normal force and friction force are acting only on the front two feet when tipping occurs. The normal force on each of the front feet is half of the total vertical force. The four normal forces are all equal since the counterweights goal is to make the center of mass in the middle of structure to prevent tipping. This would result in an evenly distributed normal force. The static friction force is determined by this equation

$$F_f < \mu_{static} N \tag{9.1.3}$$

where F_f is the friction force, μ is the friction coeffiecnt, and N is the normal force. The friction coefficient that is being used for the analysis is between dry concrete and steel. The value was μ equal to 0.57 [30]. The last force will be a counterweight to go against the tipping of the arm and actuation.

The free body diagram of the rigid body can be seen in Figure 9.1.2. The x axis is to the right, the y axis is vertical, and the z axis is out of the page.

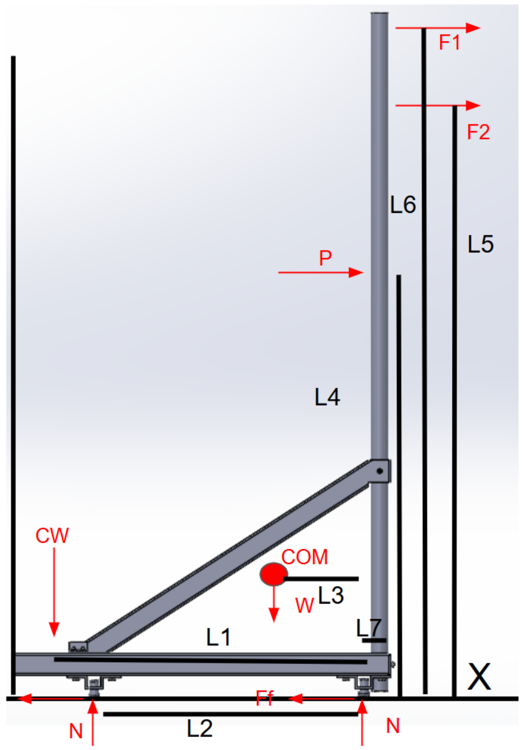

Figure 9.1.2. Free body diagram of the Structure.

The main direction that tipping can occur is about the z axis. The tipping was found about the front most edge right where the right normal force occurs. The total moment of the z axis was found to figure out the counterweight value. The counterweight denoted in Figure 9.1.2 is the mass location for the tipping analysis. The sum of forces was found in all three directions. The equation used for that was

$$\sum F = \sum m_i a_i \tag{9.1.4}$$

where F is the force, m is the mass, and a is the acceleration. The right-hand side of the equation is zero since the structure is not moving or accelerating in any direction. The equation for the sum of forces in the y direction is

$$0 = F_{y1} + F_{y2} - cw - w_{sys} + 2N_1 \tag{9.1.5}$$

where F_{y1} and F_{y2} are the forces from the arm, cw is the counterweight, w_{sys} is the weight of the structure, and N_1 is the normal force in the front two feet. There is no normal force on the back two feet. The y direction sums of forces resulted in an equation for the normal force in terms of the counterweight. The resulting equation is

$$N_1 = \frac{1}{2}(w_{sys} + cw - F_{1y} - F_{2y}) \tag{9.1.6}$$

The normal force equation is used just to find the force in each of the front feet. This force will eventually be used to find stress on the feet. The cross product was used to find the moment. The equation is

$$\bar{M} = \bar{R} x \bar{F} \tag{9.1.7}$$

where M is the moment vector, R is the vector from the point of inspection to the force, and F is the force vector. The collective sum of each moment was found. The equation for the sum of moments of the z axis at the front feet is

$$\sum M = 0 = cw(L1) + Fx1(L6) + Fx2(L5) + Fy1(L7) + Fy2(L7) - P(L4) + W(L4) \tag{9.1.8}$$

where M is the moment, cw is the counterweight, Fx is the x components of force one and two, Fy is the y components from force one and two, P is the pressure force, W is the total weight of the system, and L are the respective lengths. Using the z moment equation, the counterweight force can be found. Only the z moment was found since that was the main concern for tipping. The counterweight was found to be a value that would produce a zero moment of the z axis. The complete analysis can be seen in the Appendix. A plot of counterweight against the tipping moment is plotted in Figure 9.1.6.

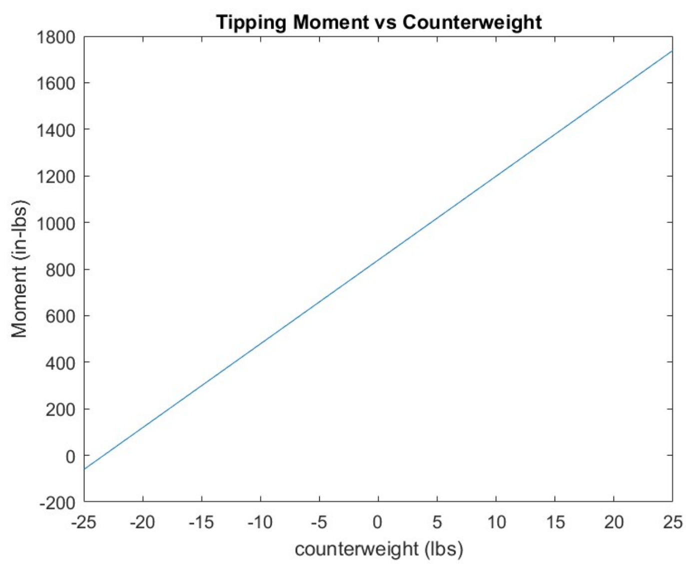

Figure 9.1.3. Plot of tipping moment against counterweight.

When the moment crosses the zero point, that is when the structure will no longer tip forward. Based on the graph, the resulting counterweight needed to avoid tipping is a minimum of -23 *lbs*. This also aligns with the value solved for in the system of equations. This means that no counterweight is needed to prevent the structure from tipping. There is an extra 800 *in-lbs* that can be applied to the structure when there is no counterweight.

9.1.2 Pole Analysis

The pole is one of the main structural elements under stress. The pole will be analyzed in two different ways. The entire pole will be analyzed without the support structure to simulate worst case scenario. The second pole analysis will be an internal cut just above the support. Both analyses will result in a force that will correspond to stress in a bolt holding the pole in place.

The entire pole will be modeled as fixed at the bottom. There will be three different force vectors acting on it. There will be F_1 and F_2 from the arm and actuator acting on the pole in addition to the pressure load from the wind gusts. The pole can be modeled as fixed due to the pole being inserted into the base and bolted in. There would be a reaction force and reaction moment in all three axes. The free body diagram of the entire pole can be seen in Figure 9.1.4.

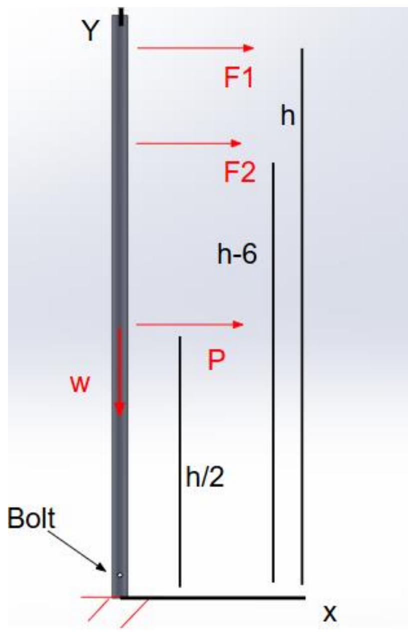

Figure 9.1.4. Free Body Diagram of the entire pole fixed.

There will be three reactions forces and three reaction moments at the base of the pole since it was modeled as fixed. The bolt location for this analysis that the stresses and moments are found about is shown in Figure 9.1.4. Using the forces and distances in Figure 9.1.4 the sum of forces and sum of moments can be found with Equation 9.1.4 and Equation 9.1.8 respectively. The resulting sum of forces and moments produce three useful equations to find the reaction force in x and y and then the reaction moment in z. The equations are

$$Fx:\ \ P + F_{1x} + F_{2x} + R_x = 0 \tag{9.1.9}$$

$$Fy:\ \ -w + F_{1y} + F_{2y} + R_y = 0 \tag{9.1.10}$$

$$Mz:\ \ M_z - \frac{Ph}{2} - F_{2x}(h-6) - F_{1x}h = 0 \tag{9.1.11}$$

where P is the force due to the wind gust, F are the forces from the arm and actuator, R is the reaction force from the fixed support, w is the weight of the pole, M_z is the reaction moment of the bolt location, and h is the total height of the pole. The three useful equations result in values for R_x, R_y, and M_z which are -4.45 *lbs*, 31.18 *lbs*, and 226.5 *in-lbs respectively*.

The resultant reactions allow for the bending stress and the bolt stress to be found. The bending stress in the pole is necessary to find out how close the pole is from yielding. The free body diagram in Figure 9.1.3 can be rotated such that the pole is now acting as a beam. Bending stress will be found using the beam bending stress equation which is

$$\sigma = \frac{My}{I} \tag{9.1.12}$$

where M is the moment induced, y is the position away from the neutral axis, and I is the moment of inertia of the cross section. The area moment of inertia for a hollow circle is defined by the equation

$$I = \frac{\pi}{64}\left(d_o^4 - d_i^4\right) \qquad \text{(9.1.13) [31]}$$

where d_o is the outer diameter and d_i is the inner diameter. Using Equation 9.1.12 and Equation 9.1.13 together the resulting bending stress can be found with is 1.15 *ksi.* This is not a major concern at all since the yield strength of the pole is significantly higher. The safety factor is roughly 35. This is significantly higher than the required safety factor, however this diameter pipe was chosen to be easily adaptable for the arm and actuation method. It gives more surface area to clamp to while producing more friction to prevent the arm from sliding.

There is a bolt at the bottom of the pole that prevents it from moving. There will be stress in the bolt due to the forces at that location. The magnitude of the reaction forces will be found and used to find the stress in the bolt. The maximum transverse shear can be found by multiplying the value by a certain factor that comes from the cross-section geometry. The equation is the

$$\tau_{max} = \frac{4}{3}\frac{F}{A_{pin}} \tag{9.1.14}$$

where τ_{max} is the maximum transverse shear in the bolt, F is the force on the bolt, and A_{pin} is the area of the bolt. The force is the magnitude of the reaction forces. The bolt has a ½ *in* diameter. The resulting transverse shear stress is 53.5 *psi*. The yield strength for the bolt that will be purchased will be quite a bit larger than the found stress. The safety factor is not a concern. The bolt location can be seen in Figure 9.1.5.

The same process that was done for the entire pole will be done for an internal cut just above the support to find the reactions forces. An internal cut is being made to find the forces that would be on the bolt. These forces will be used to find the stress in the bolt that connects the pole to support. The internal cut can be seen on Figure 9.1.5 with an additional length of c to denote the location of the cut.

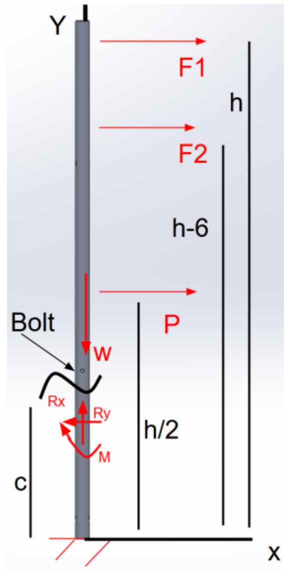

Figure 9.1.5 Free Body Diagram of the pole with an internal cut at height c.

The useful equations will be very similar to the previous case. There will be a slight difference in the y sum of forces and the moment of z. The sum of forces in the x will result in the same force found in the full pole analysis. The two new equations will be

$$Fy\text{:}\quad -\frac{w(h-c)}{h}+F_{1y}+F_{2y}+R_y=0 \tag{9.1.15}$$

$$Mz\text{:}\quad M_z-P\left(\frac{h}{2}-c\right)-F_{2x}(h-6-c)-F_{1x}(h-c)=0 \tag{9.1.16}$$

where the only new variable is c which is the location of the cut. The new values for R_x, R_y, and M_z will be -4.45 *lbs*, 24.68 *lbs*, and 87.83 *in-lbs*. These values are smaller than the previous case, which is expected since it is less of the pole and the moment arms are smaller. By following the same process of bending stress and transverse shear in the bolt, the values can be found using Equation 9.1.13 and Equation 9.1.14. The resulting bending stress is 444 *psi,* and the resulting transverse shear stress is 42.6 *lbs*. Given the material properties of the pole these values are not close to the factor of safety but exceed it by a large margin. The two-inch pole was chosen due to the large objects being attached to it from the arm and actuation method. The attachment mechanism for the arm and actuation system to the structure needs a large surface area to produce more friction to work. The clamps keeping the arm up need to be rigid and the large surface area creates more friction.

9.1.3 Feet Analysis

There are four adjustable feet on the structure. The feet need to be adjustable to ensure that the structure is level to avoid any additional tipping moments. The adjustable feet work with a nut and screw holding all the weight at each foot. Because the feet are adjustable, the stress in the bolts need to be found to ensure that the bolts do not yield and cause the structure to tip. The free body diagram can be seen in.

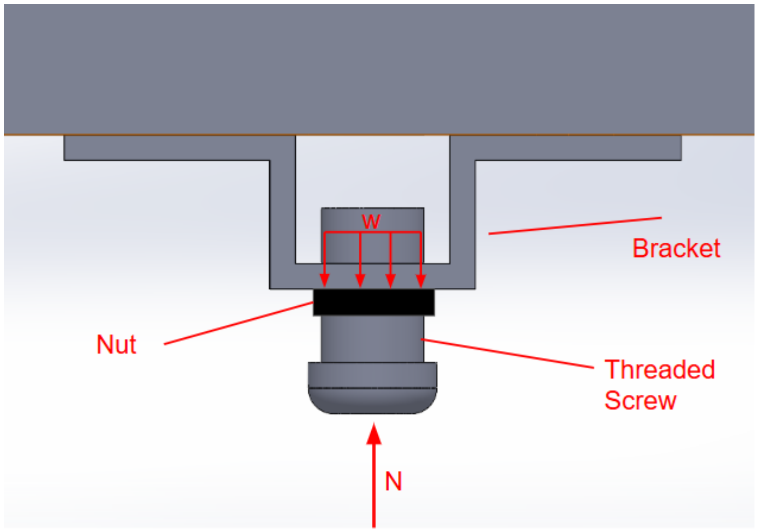

Figure 9.1.6. Free Body Diagram of the threaded screw and the nut that holds the weight.

The weight force in one of the screws will be the entire vertical force for this analysis since that is worst case scenario. Weight is the only force that needs to be considered when solving stress in the bolts. An ACME thread was used to do these calculations throughout. A ¾ *in* bolt diameter was used with a threads per inch of 6. The basic height of the thread is 0.08333 *in* [32]. The bolts will be idealized as power screws since they are holding a load on the nut. The bearing pressure on the screw can be found by

$$\sigma_{bearing} = \frac{W}{\pi d_m h n} \qquad (9.1.17)\ [32]$$

where $\sigma_{bearing}$ is the bearing pressure on top of the bolt, W is the load, d_m is the mean screw diameter, h is the depth of the thread, and n is the number of threads engaged. The number of threads assumed for this analysis that were engaged was three. The resulting bearing pressure with the ¾ *in* bolt and a ½ *in* nut is -383.39 *psi*.

The shear stress of the bolt was found

$$\tau_s = \frac{3W}{2\pi d_r h b} \qquad (9.1.18)\ [32]$$

where τ_s is the shear on the screw, d_r is the root diameter which is the diameter of the screw without the threads, and b is the beam depth. The resulting shear stress based on the same ACME bolt is -328.6 *psi*. The compressive stress was found next using

$$\sigma_c = \frac{W}{\frac{\pi}{4}\left(\frac{1}{2}(d_r + d_p)^2\right)} \qquad (9.1.19)\ [32]$$

where σ_c is the compressive stress on the bolt, d_r is the root diameter, which is the diameter with threads, and d_p is the diameter to the middle of the threads. The resulting compressive stress is -254.7

psi. The screw is short, so the buckling failure mode is not an area of concern. Now, combining compressive stress and the shear stress the maximum stress can be found using

$$\tau_m = \sqrt{\left(\frac{\sigma_c}{2}\right)^2 + \tau_s^2} \qquad (9.1.20)\ [32]$$

where τ_m is the maximum shear in the bolt. The resulting maximum shear is 352.4 *psi*. All the shear values are small and not close to the yield strength of the bolt. The bolt diameter will not change since it would make it harder to adjust the height of the structure. The bolts will be adjusted by hand in the middle of nowhere, so larger bolts will allow for easier access. Any smaller bolts would not be as accessible when the structure is fully put together in the desert.

9.2 Arm and Joint Analysis

The structural analysis of the arm and joint section of the Launch Latch is essential for maintaining stability and reliability during fueling operations. This section examines the load-bearing capacity and overall structural integrity of the arm and joint assembly, with a focus on identifying potential failure points under the combined influences of component weight, disconnect pressures, and wind forces. By evaluating each element's performance under worst-case scenarios, this analysis aims to refine the design to balance structural robustness with considerations for weight, portability, and ease of assembly, ensuring both safety and operational efficiency in the launch environment. In the following sections, an outline of the analysis will be provided, reference Appendix C which includes the MATLAB code for all explicit calculations.

9.2.1 Component and Force Definitions

Throughout the arm and joint analysis, key components are referred to using general nomenclature. Figure provides a reference for the square pipe with subscript ‘arm’, support bar with subscript ‘sup’, upper and lower clamp with subscripts ‘u’ and ‘l’ respectively. Also referenced in Figure 9.2.1 are the locations of pinned joints, A, B, and C.

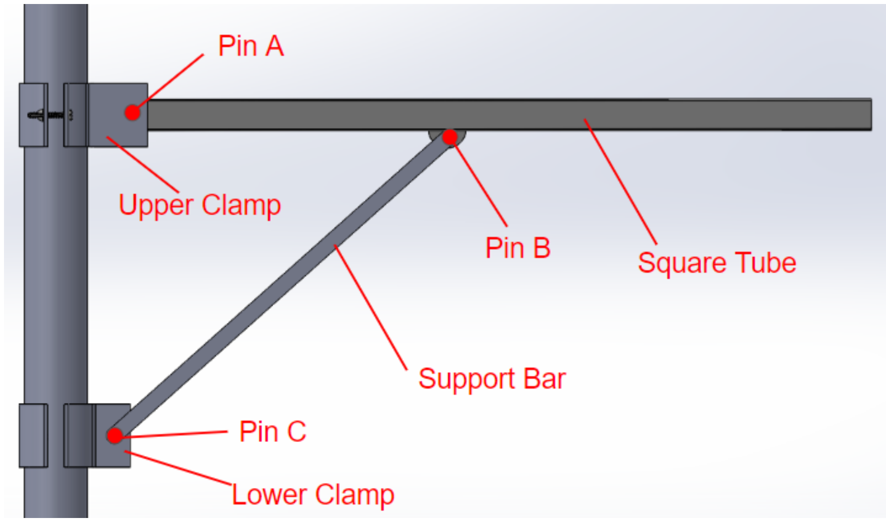

Figure 9.2.1. General Nomenclature for Arm and Joint Analysis

The analysis will be carried out for the worst-case scenario and evaluated by considering an instant in which all loads are static, representing a condition where the maximum forces are simultaneously applied. In the static load scenarios in the following sections include forces from the component weights, wind drag, and either disconnect forces during operation or handling forces during setup. Each of these forces are assumed to act concurrently and at their peak magnitudes.

The basis of the analysis is dependent on the input forces to determine optimal dimensions for the components. The following forces will govern the loading worst-case loading conditions. First, calculating the weight of the square pipe,

$$W_{arm} = \rho_m V_{arm} \tag{9.2.1}$$

where, ρ_m is the density of steel at $0.284\ lb/in^3$ according to ASTM A513 [33] and V_{arm} is the volume of the bar. The weight will act as a point load at half the length of the square tube in the negative y-direction.

Next, the drag force due to wind on the square tube is defined by equation 9.1.2, where ρ is the density of air at $1.372 * 10^{-6}\ slug/in^3$ [34]. V is the wind speed which can be 30 mph in the desert. C_d is the coefficient of drag for flow over a square tube and A is the frontal area of the square tube [29]. The force due to wind on the arm structure is approximately 0.8 *lbs* so it will be neglected for the remainder of the analysis.

The force due to valve disconnect is equal to,

$$F_{dis} = P_{N2O} A_{noz} \tag{9.2.2}$$

where, P_{N2O} is the max saturation pressure of N_2O and A_{noz} is the area of the nozzle orifice.

Additionally, the weight of the actuation system, W_{act}, is based on the actuation design and is approximately about 6 lbs acting in the negative y-direction, 44 inches from Pin A. Finally, an additional handling force, W_h, will be added to the analysis to consider the possibility of additional loading from an operator while setting up. A conservative estimate of this case is 20lbs of force exerted at the end of the square tube. The handling force and the disconnect force will never occur at the same time, and the handling force results in higher stresses so the disconnect case will be disregarded for the remainder of the analysis.

In the following sections, equations and calculations are outlined, however for more specific values, see Appendix C for the MATLAB script used to calculate explicit values.

9.2.2 Square Tube

To reduce the moment induced on to the entire structure and to save material costs, it is favorable to minimize the weight of the square tube and the support bar. For the square pipe the max stress can be assumed to be due to an internal bending moment at the support reaction, Pin B. Taking a cut of the square tube at this point can be seen in Figure 9.2.2.

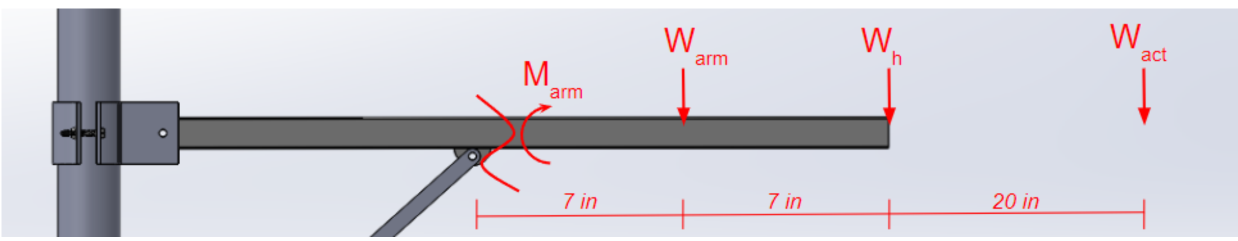

Figure 9.2.2. Free body diagram for cut of the square pipe at Pin B.

From Figure 9.2.2, the internal moment in the z-direction can be found by summing the moments about Pin C,

$$\sum M_C = 0 = M_{arm} + \sum W_i * r_{W_i/C} \tag{9.2.3}$$

where, M_{arm} is the internal moment at point C, W_i is a weight from Figure 9.2.2, and $r_{W_i/C}$ is the moment arm from W_i to Pin C. Using the value for M_{arm}, the max stress on the square tube can be found through the flexure formula,

$$\sigma_b = \frac{My}{I} \tag{9.2.4}$$

Where, σ_b is axial stress due to bending, M is the bending moment, y is the vertical distance from the cross-sectional centroid, and I is the moment of inertia.

Grade 1010 Low Carbon Steel has been chosen for its cost-effectiveness and machinability. This steel has a yield stress of 32,000 *psi* [33]. Therefore, the factor of safety is defined by,

$$FoS = \frac{\sigma_y}{\sigma_{max}} \tag{9.2.5}$$

where, FoS is the factor of safety, σ_y is the yield stress of steel, and σ_{max} is the max operating stress. This results in a factor of safety of 4.3 for a square tube of side length 1 *in* and wall thickness 16 GA.

The defined dimension for the square pipe allows for an accurate analysis of the entire square tube. Figure 9.2.3 defines the free body diagram for the square tube which is pinned to the upper clamp and support bar.

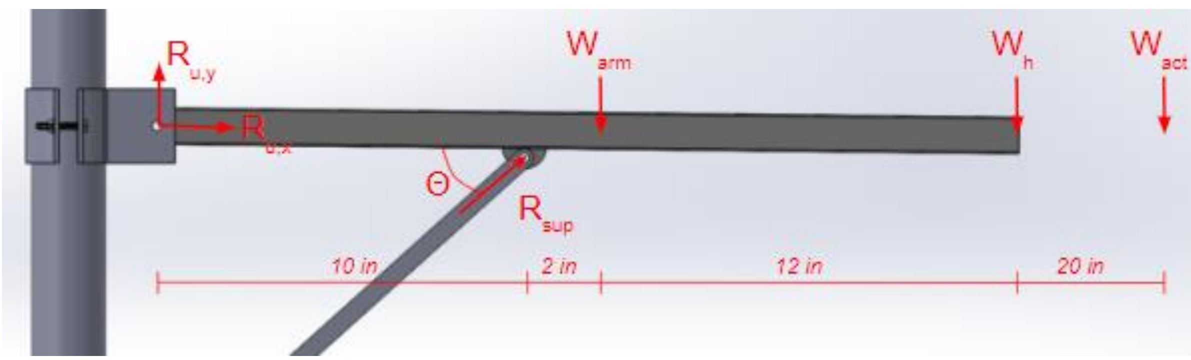

Figure 9.2.3. Free body diagram of square pipe with resultant point loads.

Where W_{arm} is the weight of the arm defined by equation 9.2.1, W_h is the additional handling force, W_{act} is the weight of the components that actuate and R_{sup} is the reaction from the support arm. Reactions, $R_{u,x}$, $R_{u,y}$, and R_{sup} from Figure can be evaluated via summing moments about R_u in the z-direction and summing forces in each defined direction.

$$\sum M_{R_u,z} = 0 \tag{9.2.6}$$

$$\sum \vec{F} = 0 \tag{9.2.7}$$

These equilibrium equations result in R_{sup} as 87.9 *lbs*, $R_{u,x}$ as -62.1 *lbs*, and $R_{u,y}$ as -33.5 *lbs*. The results for these reactions will provide a basis for further analysis on torque specifications and stresses at Pins A and B.

9.2.3 Support Bar

The support bar will feature a hollow square cross-section, with its side length and wall thickness determined based on the results of the stress analysis. The primary load will be compressive, making potential failure modes include axial yielding and buckling.

For axial yielding, the axial stress can be determined by,

$$\sigma_a = \frac{F}{A} \tag{9.2.8}$$

where σ_a is axial stress, F is the applied load, and A is the cross-sectional area. This stress can provide the factor of safety against axial yielding of the support bar by defining the factor of safety as,

$$FoS = \frac{\sigma_y}{\sigma_a} \tag{9.2.9}$$

where, FoS is the factor of safety, σ_y is the yield stress of low carbon steel, and σ_a is the actual stress in the support bar induced by the compressive load, R_{sup}.

For buckling, critical loads are governed by,

$$P_{crit} = \frac{\pi^2 EI}{(KL)^2} \tag{9.2.10}$$

where, P_{crit} is the critical load to induce buckling, E is the elastic modulus of the material, I is the moment of inertia of the member, K is an effective length of one due to the member being pinned at both ends, and L is the length of the member [35]. This critical load can provide the factor of safety against buckling of the support bar by defining the factor of safety as,

$$FoS = \frac{P_{crit}}{R_{sup}} \tag{9.2.11}$$

where, FoS is the factor of safety, P_{crit} is the critical load that would induce buckling, and R_{sup} is the compressive force on the support bar.

Limits for the compressive yield safety factor will be set to a minimum of 2 and buckling a minimum safety factor of 3. Figure 9.2.4, shows the potential dimensions for the support bounded by the defined safety factor limits.

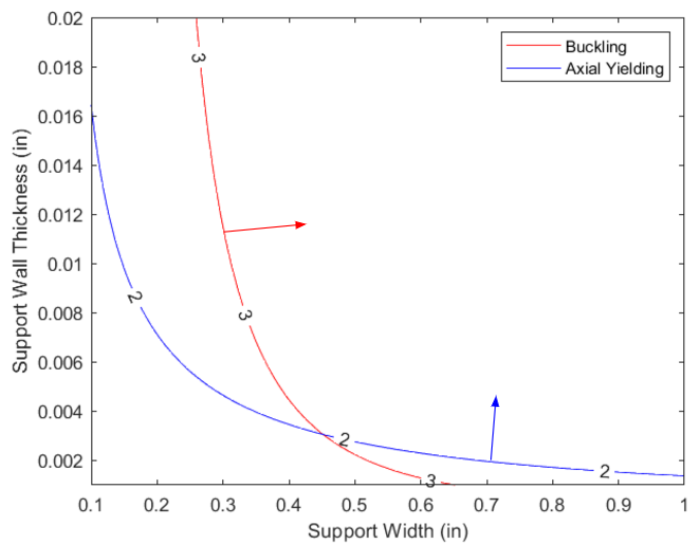

Figure 9.2.4. Potential Dimensions of the support bar with overlay of safety factor limits. Arrows point towards an acceptable region.

To minimize manufacturing costs, the design will utilize standard square tubing with a minimum support width that meets industry standards. For this design, 0.5 *in.* square tubing is selected. Based on Figure 9.2.4, it is evident that the support bar will fail to meet the required safety factor due to axial yielding before buckling occurs. To address this, the minimum wall thickness required to achieve a safety factor greater than 2 is calculated to be 0.0029 *in*. Again, to ensure manufacturability, the design will specify an 18 GA wall thickness.

Continuing on to the reactions in the support bar, R_{sup} from the analysis of the square tube and the weight of the support bar, W_{sup}, can be used to determine the reactions between the lower clamp and support bar from the free body diagram of the support bar seen in Figure 9.2.5.

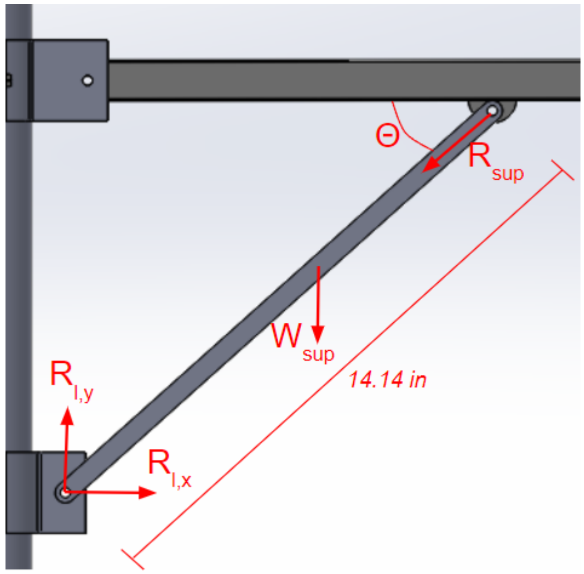

Figure 9.2.5. Free body diagram of the support bar to determine reactions at Pin C.

Summing moments about R_l in the z-direction and forces in the defined directions results in the following equilibrium equations,

$$\sum M_{R_l,z} = 0 \tag{9.2.12}$$

$$\sum \vec{F} = 0 \tag{9.2.13}$$

These equilibrium equations result in $R_{l,x}$ as 87.9 *lbs* and $R_{l,y}$ as 62.6 *lbs*. The results for these reactions will provide a basis for further analysis on toque specifications and stresses at Pin C.

9.2.4 Pinned Joints

Another potential failure point in the arm and joint is the shear stress induced on the pins at each joint due to reaction forces calculated above. Pin A will be in double shear and Pins B and C will be in single shear. The shear stresses in the two types of geometries are governed by,

$$\tau_s = \frac{VQ}{It} \tag{9.2.14}$$

and,

$$\tau_d = \frac{VQ}{2It} \tag{9.2.15}$$

where, τ_s is shear due to single shear, τ_d is shear due to double shear, V is the force in the shear plane, I is the 2nd moment of inertia, Q is the first moment of area and t is the diameter of the pin.

Evaluating the shear stress at Pins A, B, and C, as defined in Figure 9.2.1, will experience a max shear stress of 1.0 *ksi*, 2.4 *ksi*, and 1.8 *ksi*, respectively, based on the von Mises yield criterion, yield stress in pure shear is governed by,

$$\tau_y = \frac{\sigma_y}{\sqrt{3}} \tag{9.2.16}$$

where, τ_y is the yield stress due to pure shear and σ_y is the yield stress of steel in tension. [36]

The safety factor of this joint will be defined by equation 9.2.6. The resulting factors of safety for Pins B and C in single shear are 10.3 and 7.7 respectively. As for Pin A, the factor of safety has increased to 19.3 as it is in double shear. Smaller pins could be used for each joint, however, it is advantageous to use ¼ inch pin diameter for ease of assembly and for the pins to be interchangeable between all joints.

Another potential high stress area on the joints is due to the bearing stress on the pin holes at each joint. The bearing stress can be evaluated by,

$$\sigma_b = \frac{F}{A_{proj}} \tag{9.2.17}$$

where, σ_b is the bearing stress on the pin hole, F is the reaction force due to the contact with the pin, and A_{proj} is the contact area projected onto the plane normal to the reaction force. In practice the pin will not be the same diameter as the pin hole, so a conservative contact area will be estimated to be a third of the arc length of the pin hole. The resulting stresses at the contact points at Pins A, B, and C are 1.3 *ksi*, 3.2 *ksi*, and 3.3 *ksi* respectively. Applying equation 9.2.6, the corresponding factors of safety are 24.5, 9.9, and 9.8. These factors of safety show that the shear in the pins will fail prior to yielding due to bearing stresses.

9.2.5 Torque Specifications

It is necessary to ensure the arm does move from the desired height. Torques can be specified for the bolts on each clamp to ensure the clamping force is sufficient to resist slip between the clamps and the vertical post. Initially the minimum static friction force on the inner radius of a clamp can be computed through a free body diagram of the upper clamp as shown in Figure 9.2.6,

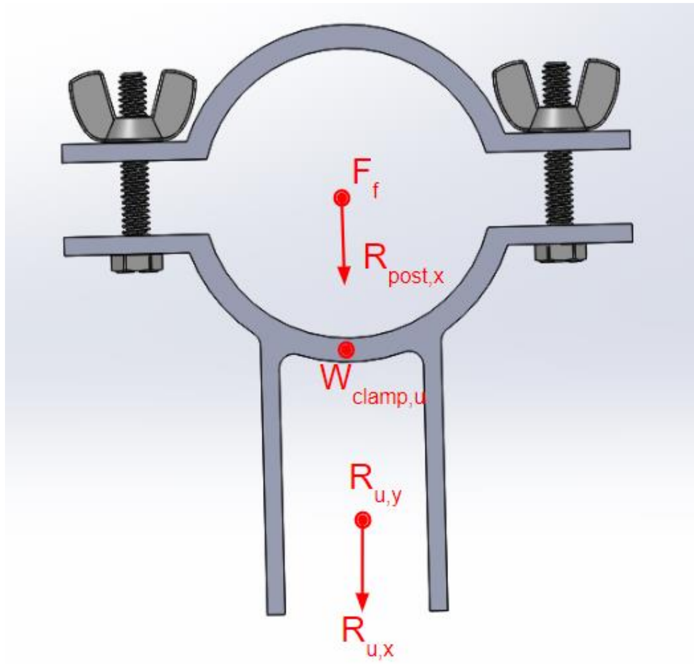

Figure 9.2.6. Free body diagram of the upper clamp to determine the required frictional force between the clamp and vertical post.

where F_f is the force due to friction between the clamp and vertical post, $W_{clamp,u}$ is the weight of the upper clamp, $R_{post,x}$ is the reaction from the post onto the upper clamp, and $R_{u,x}$ and $R_{u,y}$ are the reaction forces determined in section 9.2.2 at the pinned joint of the square tube and upper clamp. Summing these forces in the out of plane direction,

$$\sum F_y = 0 \tag{9.2.18}$$

results in a required friction force of 35.5 *lbs* to maintain static equilibrium.

Similarly for the lower clamp shown in Figure 9.2.7,

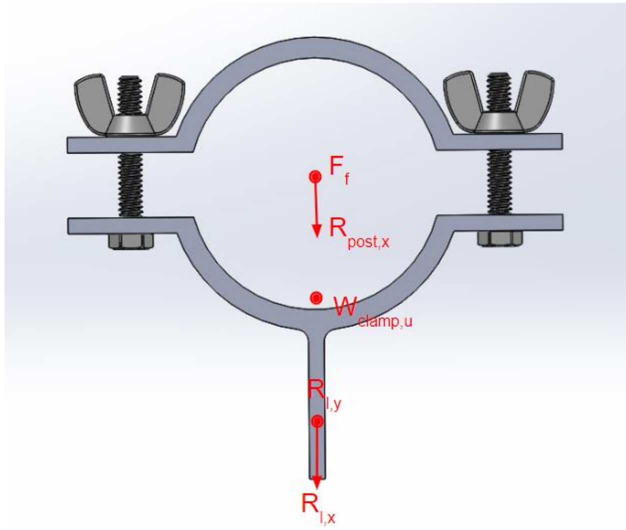

Figure 9.2.7. Free body diagram of the lower clamp to determine the required frictional force between the clamp and vertical post.

where F_f is the force due to friction between the clamp and vertical post, $W_{clamp,l}$ is the weight of the lower clamp, $R_{post,x}$ is the reaction from the post onto the upper clamp, and $R_{l,x}$ and $R_{l,y}$, are the reaction forces previously determined at the pinned joint of the support bar and lower clamp. Summing the forces in the vertical direction defined by equation 9.2.20, results in a required friction force of 60.6 *lbs* to maintain static equilibrium.

The normal forces to produce the required frictional forces are governed by,

$$F_f = \mu_s N \tag{9.2.19}$$

where F_f is the frictional force, N is the normal force between the clamp and vertical post, and μ_s is the coefficient of static friction between two, dry, steel components. This value is equal to 0.74 [37]. Now zooming in on one half of the split ring clamp as shown in the free body diagram in Figure 9.2.8 where P_{bolt} is the preload on each bolt and N, again, is the clamping force onto the vertical post.

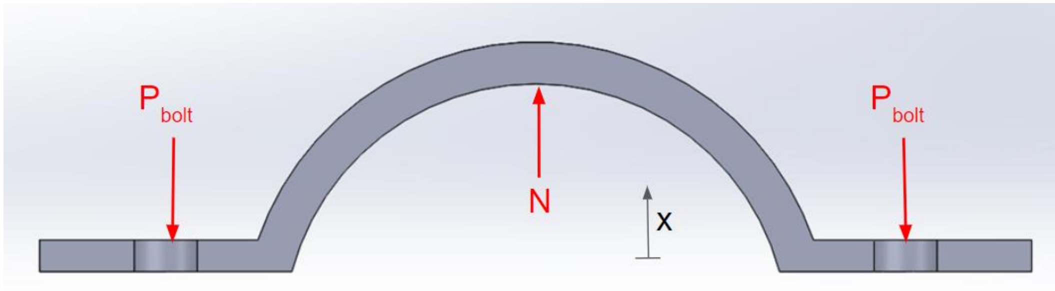

Figure 9.2.8. Free body diagram of the back half of the clamp to determine required preload.

Summing the forces in the defined x-direction,

$$\sum F_x = 0 \tag{9.2.20}$$

will determine the magnitude of P_{bolt} and using this, the required torque of each bolt can be computed using the toque-tension equation,

$$T = KDP_{bolt} \tag{9.2.21}$$

where T is the toque of the bolt, P_{bolt} is the preload on the bolt, and K is the 'nut factor' which depends on surface finish, lubrication, and thread type. From ASTM A193, an approximate nut factor of 0.20 will be used for dry conditions [38]. The required toque to ensure no slippage is 1.8 *in-lbs* for each bolt on the top clamp and 3.1 *in-lbs* for the bolts on the lower clamp. The design will specify that all bolts to be torqued to 6 *in-lbs*. Approximately 10 *in*-lbs is achievable via a wing nut tightened by hand, therefore this will be a sufficient method of torquing.

In conclusion, the structural analysis of the arm and joint assembly confirms the design's stability under worst-case loading conditions. The evaluation of forces, including weight, wind drag, and disconnect forces, ensures safety during fueling operations. The findings, including factors of safety for key components, show a robust design with optimized dimensions that balance weight, strength, and ease of assembly. This analysis provides a solid foundation for refining the design and ensuring operational reliability and efficiency.

9.3 Actuation Analysis

The actuator is essential in ensuring all sensitive components are clear of the exhaust plume left by the rocket. The plume is caused by hot gas shooting out of the end of the rocket upon launch, which imposes a high thermal load on anything in its direct line of fire. As the actuator is spring-driven, the possibility of vibrational problems cannot be ignored. This section examines the fuel plume using qualitative analysis and a 1-D transient conduction simulation, frictional analysis to determine the minimum spring constant, and solution of the coulomb damping system to determine the optimal spring constant.

9.3.1 Thermal Analysis

First, qualitative analysis was performed to estimate the size of the exhaust plume for the Half Cat Mojave Sphinx rocket. Secondly, combustion analysis was performed to characterize the temperature of gas upon exiting the rocket. Finally, a transient numerical simulation was created to determine a temperature profile outside of the fuel plume.

Through inspection of launch photos and videos, the diameter of a typical launch plume can be determined. As the height of the Mojave Sphinx is known, simple geometry and image analysis can be employed to characterize the size of the plume. The result of this analysis is outlined in Figure 9.3.1.

Figure 9.3.1: Breakdown of Fuel Plume Width Before Launch Rail Departure [14]

From this image analysis, it can be determined that, after nominal separation from launch rail, the width of the fuel plume is roughly 60 inches, which requires our actuation system to retract 30 inches to be clear of the fuel plume.

To further characterize the launch plume, NASA CEA (Chemical Equilibrium Applications) was used to run combustion analysis. CEA uses chemical equilibrium thermodynamics to determine the state and composition of gasses created by propellant combustion in rocketry and gas dynamics problems [39]. Using Isopropanol fuel and Liquid Nitrous oxidizer, an adiabatic flame temperature T_0 of $3028°F$ $(1938°K)$ is determined, as well as the chemical makeup of the combustion products, outlined in Table 9.3.1.

Table 9.3.1: Mole Fractions of Gases Determined by NASA CEA

Species	**Mole Fraction**	**Specific Heat Ratio, γ**
CO	0.264	1.4
CO2	0.0224	1.26
H2	0.297	1.405
H2O	0.110	1.32
N2	0.305	1.4

Next, the exit temperature of the gas must be determined, which requires the specific heat ratio of the mixture of gases. Using,

$$\gamma_{tot} = \sum_{i=1}^{n} M_i \gamma_i \tag{9.3.1}$$

where γ_{tot} is the combined specific heat ratio, M_i is the mole fraction of gas i, and γ_i is the specific heat ratio of gas i [40]. γ_{tot} is found to be 1.387. Now, gas dynamics can be utilized to find the Mach number at the exit plane. Using,

$$\left(\frac{p_e}{p_0}\right)^{\frac{1-\gamma}{\gamma}} - 1 = \frac{\gamma - 1}{2} M_e^2 \tag{9.3.2}$$

and,

$$\frac{T_e}{T_0} = \left(1 + \frac{\gamma - 1}{2} M_e^2\right)^{-1} \tag{9.3.3}$$

Where p_e is the ambient pressure, p_0 is the combustion (stagnation) pressure, T_e is the exit temperature, T_0 is the adiabatic flame temperature, γ is the specific heat ratio, and M_e is the Mach number at the exit [40]. M_e is found to be 2.54 and T_e is found to be $1109°F$ $(871.96°K)$.

Finally, using this data, a numerical transient 1-D radial heat transfer simulation was constructed. The purpose of this simulation is to ensure that the temperature from the gas plume will not conduct outward through the air and cause warping to any structural sections or damage to electronics. While air is a poor conductor of heat, components being close to the fuel plume for any period of time runs the risk of being affected.

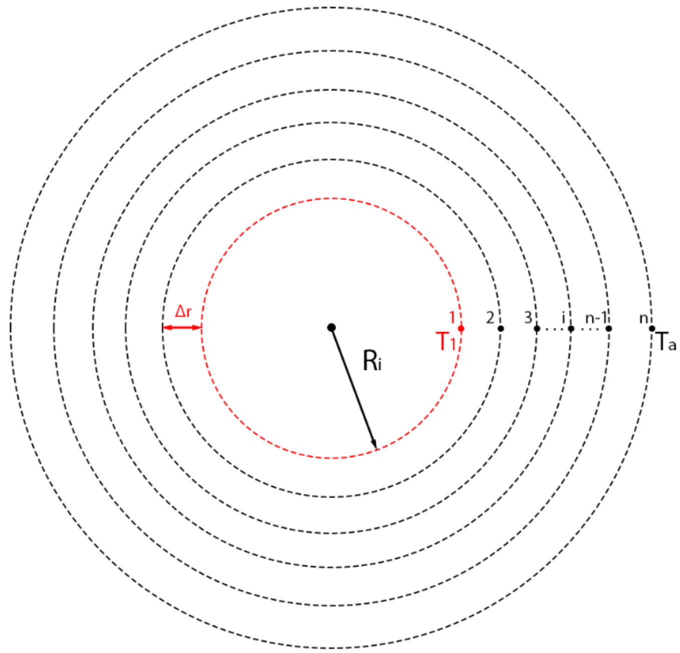

Figure 9.3.2: Transient Numerical Heat Transfer Simulation Layout

The system (shown in Figure 9.3.2) can be described as a hollow cylinder split into *n* distinct segments of size Δr. The inner boundary is fixed at T_1 to describe the fuel plume temperature, and the outer boundary is fixed at T_a, the ambient temperature. It is assumed that effects from convection and radiation are negligible, and the only form of heat transfer is conduction through air. As this is a transient simulation, each node also stores energy. The energy balance for node i is detailed in Figure 9.3.3.

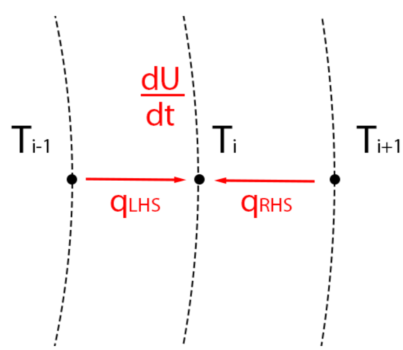

Figure 9.3.3: Energy Balance Diagram for Node i

Using this energy balance, the following equation can be found:

$$q_{LHS} + q_{RHS} = \frac{dU}{dt} \tag{9.3.4}$$

By using,

$$q = \frac{\Delta T}{R} \tag{9.3.5}$$

And,

$$R_{cyl} = \frac{\ln\left(\frac{r_{out}}{r_{in}}\right)}{2\pi L k} \tag{9.3.6}$$

And,

$$\frac{dU}{dt} = V\rho c \frac{dT}{dt} \tag{9.3.7}$$

Where q is energy transfer rate, ΔT is the change in temperature between nodes, R is the thermal resistance, R_{cyl} is the thermal resistance of a cylindrical pipe in 1D radial conduction, r_{out} is the outer radius, r_{in} is the inner radius, L is the length of the pipe, k is the thermal conductivity of the medium, $\frac{dU}{dt}$ is the time rate of change of stored energy, V is the volume of the section, ρ is the density of the medium, c is the specific heat capacity of the medium, and $\frac{dT}{dt}$ is the time rate of change of the node temperature [41], an expression for $\frac{dT}{dt}$ at node i:

$$\frac{dT_i}{dt} = \frac{2k}{\ln\left(\frac{r_{out}}{r_{in}}\right)\rho c\left(r_{out}^2 - r_{in}^2\right)}\left(T[i-1] + T[i+1] - 2T[i]\right) \tag{9.3.8}$$

With the boundary conditions, equation 9.3.8, and the properties of air being $c = 1.006\frac{J}{kg-K}$, $k = 0.02435\frac{W}{m-K}$, $\rho = 1.276\frac{kg}{m^3}$ at STP [42], and the ambient temperature being $90°F$, the temperature distribution can be solved for at different times, which can be seen in Figure 9.3.4.

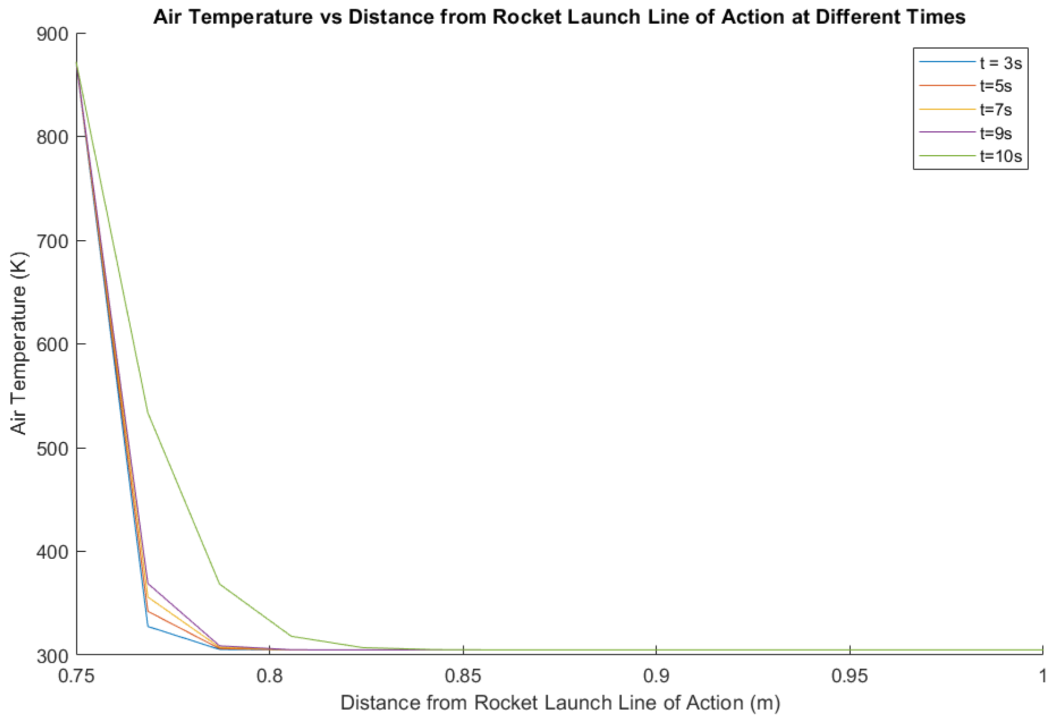

Figure 9.3.4: Air Temperature Distribution at Different Times.

As can be seen from the figure, air temperature does not increase notably outside of roughly 2 inches (5cm) from the fuel plume, even after an excessive burn time of 10 seconds. Thus, as long as the fuel plume is cleared, thermal effects from the plume are not a concern. Therefore, the project will be moving forward with an actuation stroke length of 2.5ft.

9.3.2 Frictional and Vibrational Analysis

As the actuation is spring-loaded, the minimum spring constant required to cause motion in the actuator must be found. A preliminary CAD mockup of the actuation system is provided in Figure 9.3.5. The collar is where the square tubing and standoff bar meet and slide along each other, and is where our friction analysis will take place. By modeling the actuation collar as a momentless rigid body, the free body diagram in Figure 9.3.6 can be found.

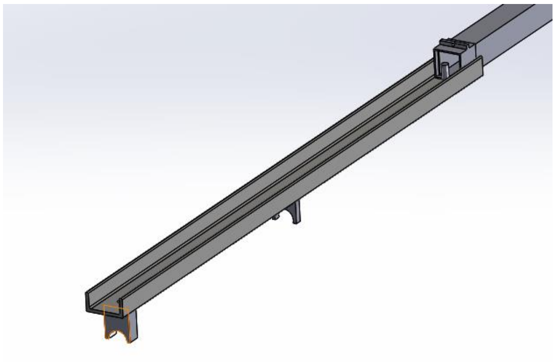

Figure 9.3.5: Actuator CAD Mockup

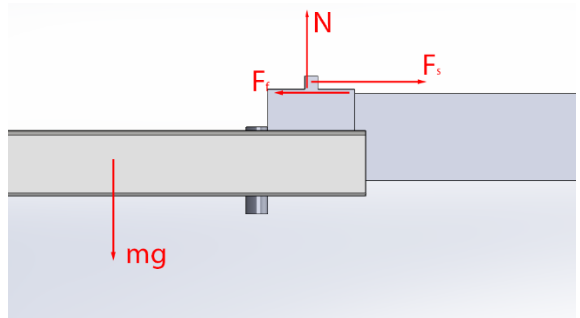

Figure 9.3.6: Actuation Collar Free Body Diagram

Where F_f is the friction force, F_s is the spring force, mg is the weight of the actuator, and N is the normal force. By summing the forces, in the y direction, $N = mg$, and by summing the forces in the x direction it can be found that,

$$kx \geq W_{actuator}\mu_s \tag{9.3.9}$$

Where $W_{actuator}$ is the weight of the actuator, μ_s is the static friction coefficient for steel sliding on steel, k is the spring constant, and x is the distance from the stop at the back end of the bar. This configuration can be seen in Figure 9.3.7.

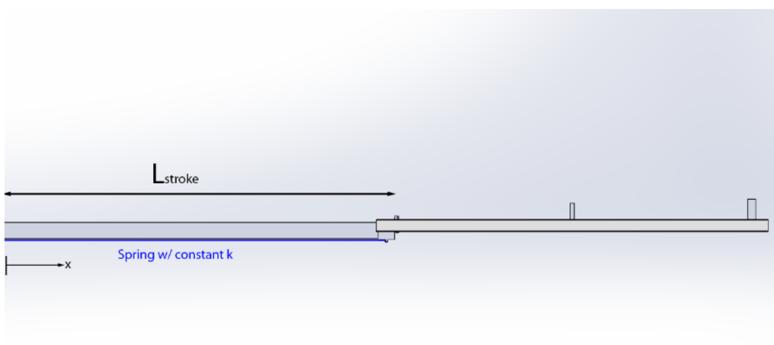

Figure 9.3.7: Actuator Collar and Bar Configuration

Using equation 9.3.7, and the coefficients for steel sliding on steel ($\mu_s = 0.8, \mu_k = 0.42$ [43]) , k_{min} , the minimum spring coefficient to achieve motion can be solved to be $k_{min} = 1.2\frac{lbf}{ft}$.
Now, it must be assured that the retraction process takes no longer than 5 seconds. By applying Newton's 2nd law, the differential equation of motion for the system can be found:

$$\frac{d^2x}{dt^2} + \frac{k}{m}x = \mu_k g \tag{9.3.10}$$

Where m is the mass of the actuation collar, and g is the universal gravitational constant. This equation was then solved using MATLAB's ode45 function to provide x as a function of time for different values of k. The plot of these values can be seen in Figure 9.3.8.

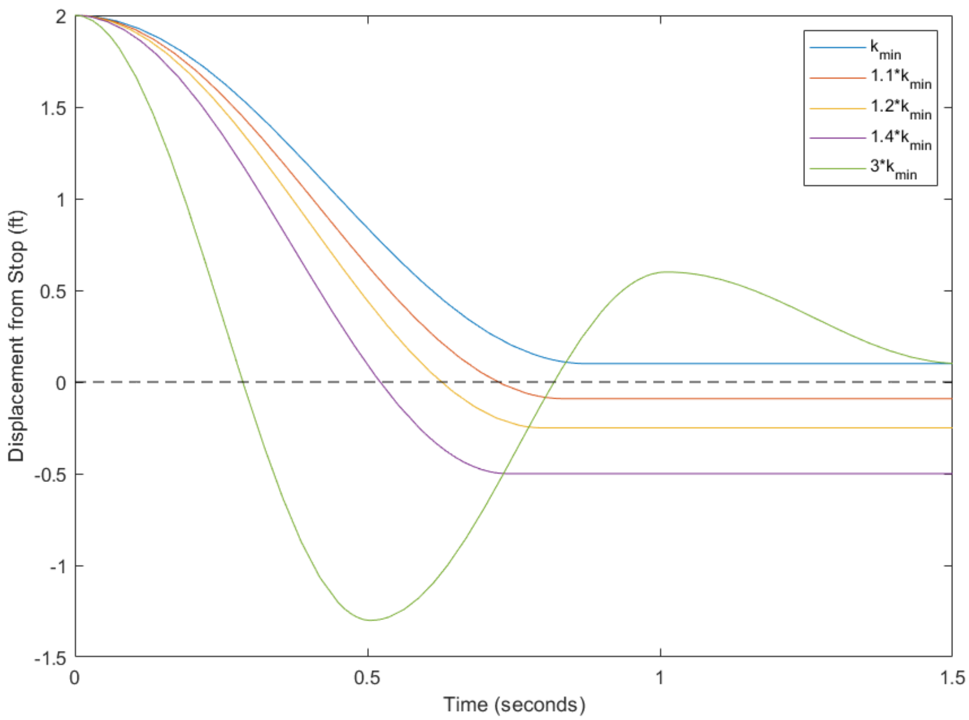

Figure 9.3.8: Displacement vs Time for Different Values of k

Due to coulomb damping, for low enough values of k the vibration system does not oscillate. Even the lowest permissible spring constant will provide sufficient speed on retraction. This is desirable, as vibrations cause additional instability in the system. However, if the system is predicted to halt after the stop, the stop will have to inflict an impulse to the standoff bar to bring it to a halt. This can cause additional shocks to the structure that can be otherwise avoided. Thus, a spring will be used with a k value between k_{min} and $1.2k_{min}$ to minimize drawback time without imposing unnecessary impulses on the system.

In summary, through the analysis of the fuel plume and the actuator, the fuel plume width, stroke length, minimum spring constant, and retraction time have been determined. These values are summarized in Table 9.3.2.

Table 9.3.2: Summary of Actuator Analysis

Quantity of Interest	Result
Fuel Plume Max. Width	$60in$
Stroke Length	$30in$
Minimum Spring Constant	$1.20\frac{lbf}{ft}$
Minimum Retraction Time	$approx. 0.75s$

9.4 Valve Analysis

The quick disconnect (QD) system is the interface between oxidizer plumbing inside the rocket and ground support equipment, seals each of these systems when disconnected, allows flow when the male and female components are connected, and seals one to the other to prevent fluid loss. A section view of the QD system is shown below in Figure for reference.

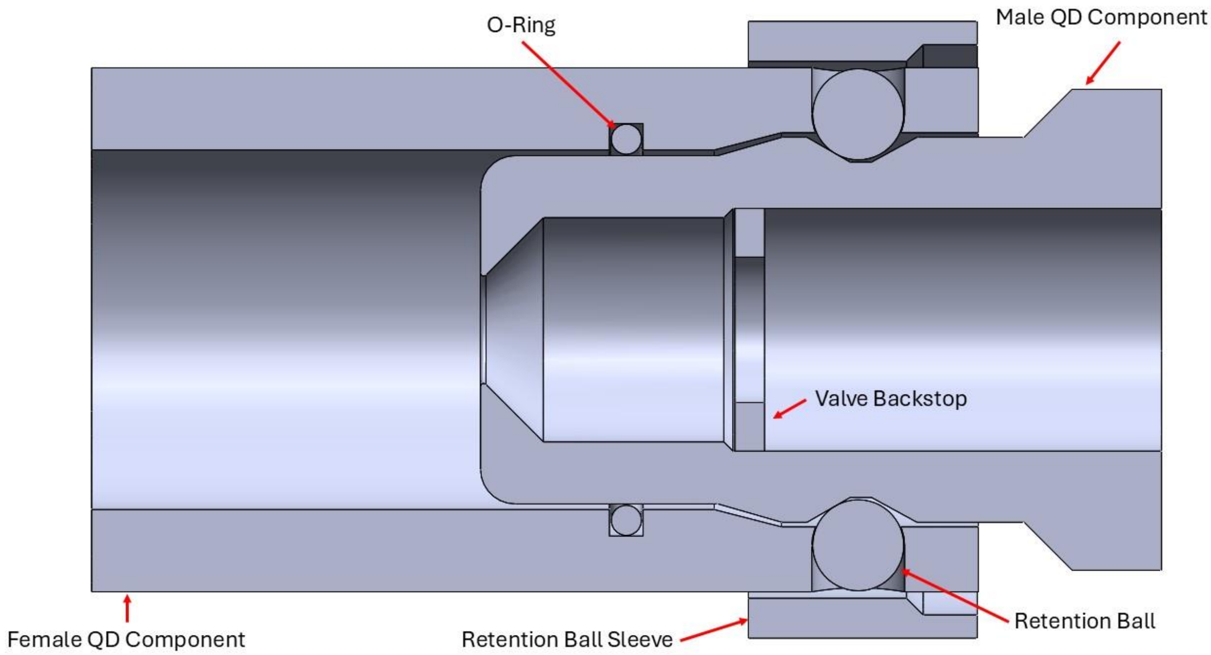

Figure 9.4.1: Annotated section view of QD system

9.4.1 Retaining Ball Detent

The male and female QD components are prevented from separating under pressure by retaining balls set in holes drilled into the female QD component. A taper at the bottom of the holes prevents the balls from falling inward when the male component is removed. An outer sleeve rides on the external surface of the female component, preventing the balls from falling outward. Depending on the position of the sleeve, the balls either have sufficient play to allow the male component to be inserted/removed, or fully constrained, locking the male component in place. A free body diagram illustrates the forces placed on the balls when the male and female components are pulled apart by system pressure

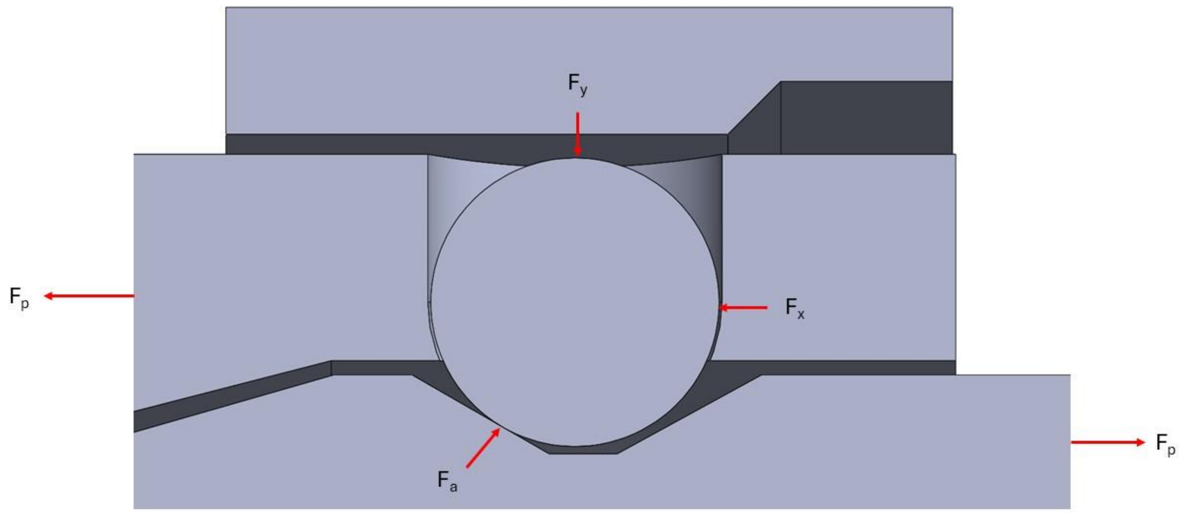

Figure 9.4.2: Free body diagram, ball detent

The lateral force on each ball $\mathrm{F_x}$ is given by the equation

$$\frac{\mathrm{F_p}}{\mathrm{n}}\mathrm{SF} = \mathrm{F_x} \tag{9.4.1}$$

where SF is the safety factor, n is the number of balls used, and $\mathrm{F_p}$ is the force pulling the components apart. $\mathrm{F_p}$ in turn can be conservatively estimated by

$$F_p = P_{OX}\pi r^2 \tag{9.4.2}$$

where P_{OX} is the oxidizer pressure, which for purposes of this analysis sits at 1000 *psi* and r is the internal radius of valve components. In this case r=0.125 *in*. Using a safety factor of 3 and 10 balls gives $\mathrm{F_x} = 49$ *lbs*.

There are three surfaces in contact with each ball. To determine the one most likely to experience failure, it consider the angle at which F_a encounters the ball θ. Balancing forces in the X and Y directions, yields

$$F_a \sin\theta = F_x \tag{9.4.3}$$
$$F_a \cos\theta = F_y \tag{9.4.4}$$
$$F_a = \frac{F_p}{\sin\theta} \tag{9.4.5}$$

$$F_y = \frac{F_p}{tan\,\theta} \tag{9.4.6}$$

The limiting case is necessarily F_a for angles shallower than 45°. θ is preliminary set at 30°, resulting in $\mathrm{F_x} = 98\ lbs$. The interaction between a sphere and a plane is described by the following three equations, taken from Roark's Formulas for Stress & Strain, table 33, case 2a [44].

$$C_E = \frac{1-\nu_1^2}{E_1} + \frac{1-\nu_2^2}{E_2} \tag{9.4.7}$$

$$\sigma_{c,max} = 0.918\sqrt[3]{\frac{P}{K_D^2 C_E^2}} \tag{9.4.8}$$

$$K_D = D_2 \tag{9.4.9}$$

Where D_2 is the diameter of each ball, which is set by ISO-7241 part B at 0.156 *in.* The QD components are preliminarily specified as 304 Stainless Steel for corrosion resistance. Per MatWeb, $E_1 = 28{,}000{,}000$ *psi* and $\nu_1 = 0.29$ [45]. The detent balls are 440C stainless steel for corrosion resistance and high hardness, $E_2 = 30{,}000{,}000$ *psi* and $\nu_2 = 0.283$ [45]. $\sigma_{c,max} = 918{,}000\ psi$, predicting localized yielding in even the stronger 440C whose yield stress is 186,000 *psi* [45].

9.4.2 Male Component Deformation

The male and female QD components will need to maintain a sliding fit, and the valve backstop is mounted in the male component by means of an interference fit. For both of these scenarios, it is important to establish the level of deformation expected under pressure.

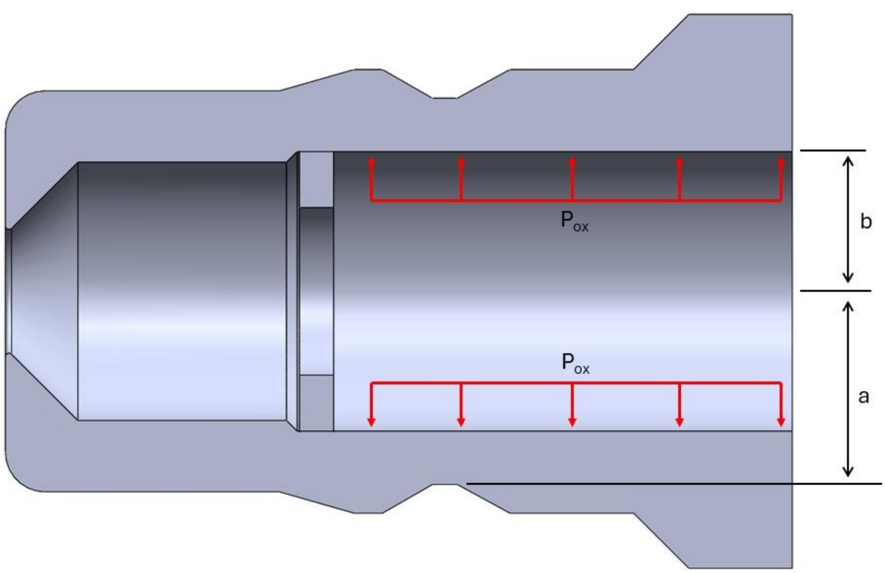

Figure 9.4.3: Free body diagram, male QD component

The male component can be modeled as a thick-walled pressure vessel, because although the walls are literally thin, they are thick in comparison to the inner and outer radius. Refer to Roark, table 32, case 1b [44].

$$\Delta \mathrm{a} = \frac{qa}{E} \frac{b^2(2-\nu)}{a^2-b^2} \tag{9.4.10}$$

$$\Delta b = \frac{qb}{E} \frac{a^2(1+\nu)+b^2(1-2\nu)}{a^2-b^2} \tag{9.4.11}$$

Where $\mathrm{a} = 0.28$ *in*, and $b = 0.19$ *in*. The pressure $Q = P_{OX}$. Referring back to the material properties in section 9.4.1, it is found that $\Delta\mathrm{a} = 1.46\text{E-}5$ *in* and $\Delta\mathrm{b} = 1.87\text{E-}5$ *in* deformations well below the tolerances in even the most sensitive slip fits, which are on the order of 1E-4 *in*.

9.4.3 Valve Backstop Retention Force

The press-fit backstop must resist spring forces imposed on it by the compression of the spring holding the internal valve shut in the disconnected configuration (not pictured). It's resistance to displacement is a function of frictional forces generated by the compression of the backstop and expansion of the male component, each by the amount of radial interference

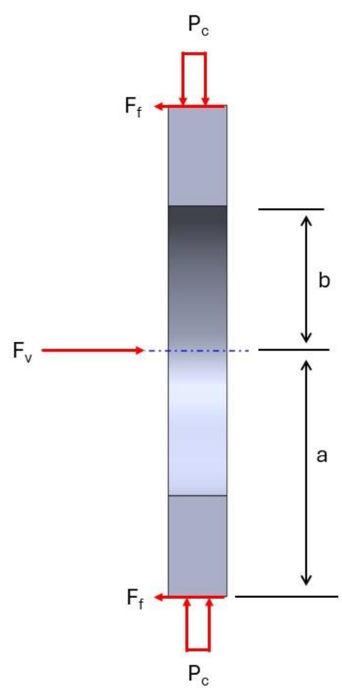

Figure 9.4.4: free body diagram, backstop friction

The backstop is also modeled as a thick-walled pressure vessel, albeit one facing external instead of internal pressure. Refer to Roark, table 32, case 1c [44].

$$\Delta a = \frac{-qa}{E}\left(\frac{a^2 + b^2}{a^2 - b^2} - \nu\right) \tag{9.4.12}$$

The sum of absolute displacement in equations (9.4.11) and (9.4.12) is set equal to the required displacement to enable the fit. A very conservative minimal radial interference of 0.00015 *in* was chosen for this analysis to compute the lowest possible retaining force. The interference pressure q =5281 *psi*. The ability of the fit to resist removal is laid out in Machine Design: An Integrated Approach, equation 7.2d [46].

$$F_f = \mathrm{F}\frac{S_{us}}{3S_{yc}} \tag{9.4.13}$$

Where S_{us} is the material's ultimate shear strength, and S_{yc} it's compressive yield strength, and S_{ut} it's ultimate tensile strength. In 304 stainless steel (used for both components), S_{ut}=73,200 *psi* [45]. $S_{us} \cong 0.8S_{ut}$

9.5 Fluid System Analysis

To characterize the fluid system for this project, some analysis needs to be carried out on the various components of the system as well as the system as a whole. This will include structural and failure mode analysis of the tubing used to ensure safety of the system, as well as thermodynamic analysis to characterize fluid flow and temperature requirements to analyze performance of the fluid system.

For a fluid system capable of safely dumping the loaded propellant into a tank, there are two primary designs characterized by the destination of the dumped propellant: one that dumps loaded oxidizer into a separate dump tank ("dump tank", Figure 9.5.1), and one that flows oxidizer back into the source tank from which the rocket tank was originally filled ("backflow", Figure 9.5.2).

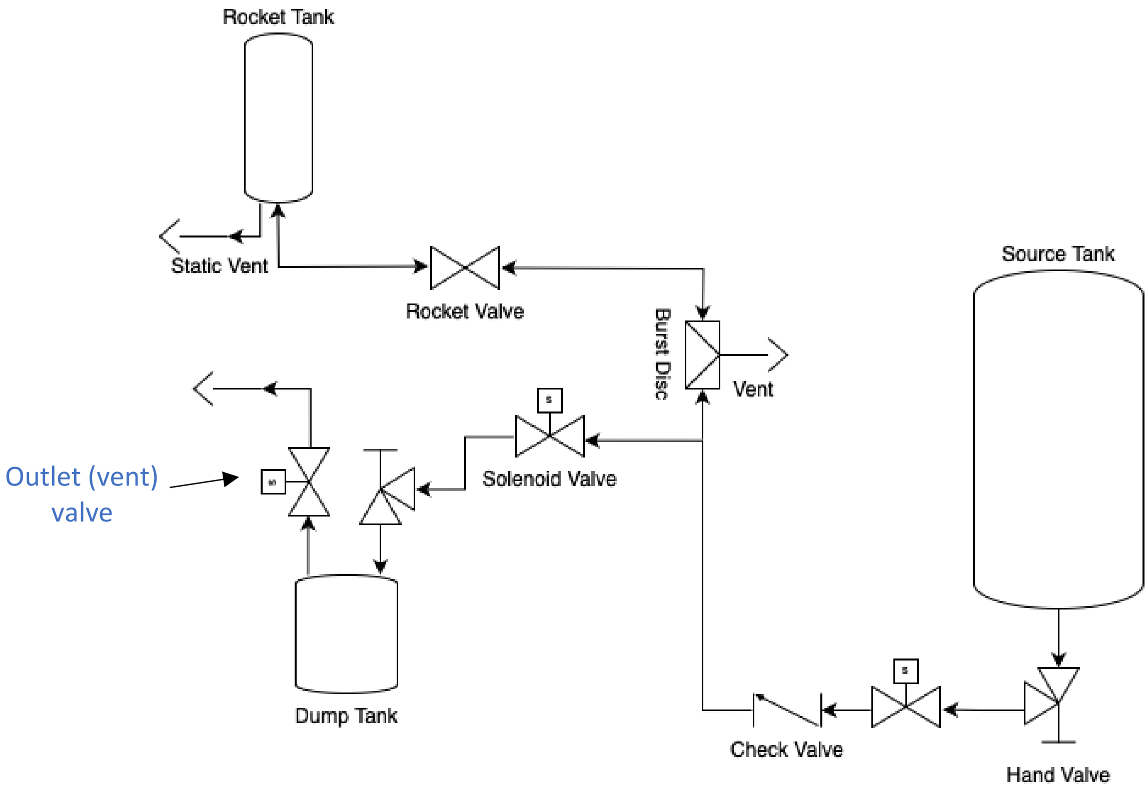

Figure 9.5.1. Piping and Instrumentation Diagram (P&ID) for a fluid system with a separate dump tank.

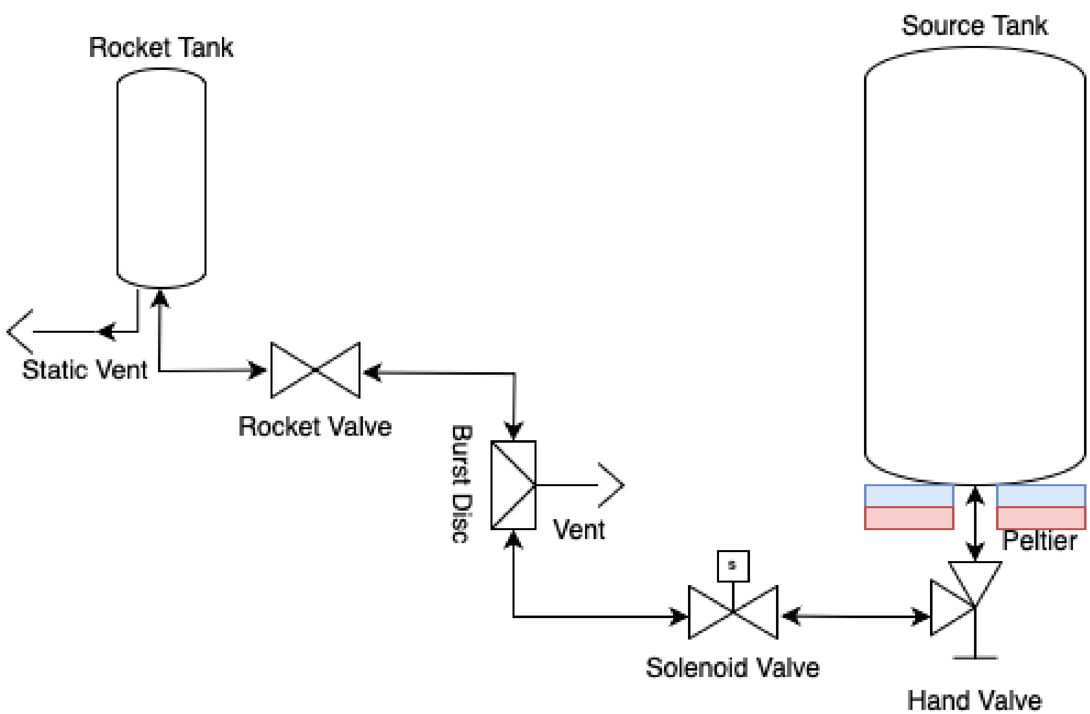

Figure 9.5.2. Piping and instrumentation diagram for a fluid system that flows back into source tank.

Comparing these two systems, the dump tank system offers a simpler and less risky solution, since it does not require flowing potentially contaminated oxidizer back into the source tank. However, it is also less performant, since the dumped oxidizer requires additional steps to be used and partially boils off in the process. In contrast, the backflow system carries with it the hazard of oxidizer contamination, but if mitigated can offer a much better system with superior performance. Because of this, the backflow system will be considered for further analysis in order to better characterize the more complex system.

9.5.1 Fluid Flow Analysis

In order for fluid (oxidizer in this case) to move from one vessel to another, there must be a pressure differential to drive the flow. The fact that the main oxidizer intended for use in this project is nitrous oxide, stored as a saturated liquid, presents a challenge for maintaining a pressure differential. Namely, N_2O's saturation pressure is remarkably high, and as such it self-pressurizes to high pressure by boiling off whenever the pressure drops. As a result of these facts, the two fluid systems presented utilize unorthodox methods of driving flow.

For a fluid system where oxidizer flows into a separate dump tank, as shown in Figure 9.5.1, the driver of flow from the rocket tank is a vent, actuated via remotely controlled solenoid valve. In the event of an abort sequence, the solenoid valve nearest the source tank will close, and both the dump tank inlet and outlet (vent) solenoid valves will open, and will close once all oxidizer has evacuated the rocket tank. This system's behavior can be estimated by inspection and determined experimentally, since the actual flow rates and times will vary significantly depending on the components used. As such, a thermodynamic analysis is not necessary at this point in time. Rather, a transient fluid analysis could be carried out should this system be chosen.

Alternatively, for a fluid system in which oxidizer flows back into the source tank, as shown in Figure 9.5.2, venting the large source tank is not feasible as 1.) it would require a (likely custom built) vessel with ports on the bottom and top, and 2.) the large volume of saturated nitrous oxide in the source tank will quickly boil off and repressurize, severely limiting the flow rate into the tank. As such, to drive flow back into the source tank, the best way to reduce the pressure is by cooling the tank, since the saturation pressure of N_2O is dependent on temperature. To calculate the required cooling to achieve desired pressure drop, thermodynamic analysis was carried out.

9.5.2 Thermodynamic Analysis

A thermodynamic analysis was run on the fluid system using the process and relations outlined below. These equations and thermodynamic properties were evaluated using Engineering Equation Solver (EES) to calculate the presented values.

First, the change in temperature in the source tank necessary to drive flow depends on the pressure drop in the fluid system. While an exact estimate of the pressure drop requires knowledge of all tubes and components in the fluid system that are outside the scope of this project, as well as ambient conditions at the launch site, an approximate value can be determined by using an online calculator, which utilizes pipe friction correlations to calculate a value. This pressure drop estimate comes to 37.5

psi or around 5% of rocket tank pressure. Iteration was done to determine the necessary temperature change to drop the saturation pressure by that same amount. It was determined that a 10°C (18°F) change in temperature of the source bottle of saturated nitrous oxide was sufficient.

To achieve the desired change in temperature in the source tank, first the heat transfer can be quantified using the mass of the tank and the initial and final enthalpies of the fluid

$$Q_{cooling} = m * (h_{final} - h_{initial}) \tag{9.5.1}$$

where $Q_{cooling}$ is the required energy loss, m is the mass of oxidizer tank, $h_{final}$is the final enthalpy of oxidizer tank after temperature change, and $h_{initial}$ is the final enthalpy of oxidizer tank after temperature change to obtain a required cooling of -280.4 *kJ* [41]. This heat transfer requirement can then be combined with the cooling ability of Peltier (thermoelectric) coolers on the bottom surface of the oxidizer bottle, where a cooling time can be determined, first by geometric inspection to determine the number of coolers from the areas

$$n_{peltier} = A_{cylinder}/A_{peltier} \tag{9.5.2}$$

where $n_{peltier}$ is the number of Peltier coolers, $A_{cylinder}$ is the bottom area of the oxidizer cylinder $A_{peltier}$ is the area of a Peltier cooler. Then the time t to cool oxidizer bottle by a desired amount can be found

$$t = Q_{cooling}/(\dot{Q}_{peltier} * n_{peltier}) \tag{9.5.3}$$

using the previously determined values and $\dot{Q}_{peltier}$, the heat transfer rate of single Peltier cooler. The time can be found to be 211 *s*, using 9.2 *W* commercially available Peltier coolers [47]. For comparison, opening the main propellant valves can empty the tank in around 10 seconds, and in the worst case the tank will slowly vent off over the course of around 3 hours. 211 seconds, or just over 3 minutes, is sufficiently quick to empty the rocket tank of the pressurized oxidizer in a controlled and less wasteful and hazardous manner. The values above were obtained in EES, using the equations above and thermodynamic properties. The code used can be found in Appendix B: EES Thermodynamic Analysis.

9.5.3 Failure Analysis

Failure modes for the fluid system can be associated with three categories: pressure, leak, and temperature. In the case of pressure failure, the pressure held within the valve, tube, or other component overcomes the strength of the component and results in some sort of burst failure.

Stresses in the rigid sections of tubing (1/4" stainless steel) can be calculated as a thin-walled cylindrical vessel with uniform radial pressure. The hoop stress is shown to be

$$\sigma_2 = \frac{qR}{t} \tag{9.5.4}$$

where σ_2 is the hoop stress, q is the uniform radial pressure (maximum for N_2O around 1000 psi), R is the radius of the tube (1/8" for 1/4" tubing), and t is the tube thickness (0.028" for 1/4" stainless tubing) [44]. This comes to around 4.5 *ksi*, well below the yield strength of 304 stainless steel (around 30 *ksi*). As a result, failure due to yield in the tubing is unlikely, with a safety factor of around 6.7.

Leak-related failure can be identified by visible liquid leaking from a connection point, or by gas forming bubbles in leak-indicator fluid. This will be analyzed experimentally during pressure and leak testing. Temperature failures can occur when, as a result of the fluid flow or other factor, a component of the fluid system becomes too hot or too cold, resulting in embrittlement or yielding and ultimately pressure failure. This is not a concern for operation in ambient conditions (design temperature range of 0°F to 120°F).

9.6 Analysis Conclusion

This analysis successfully evaluated the launch latch system, providing critical insights into its performance, safety, and reliability. By examining various factors, including mechanical, fluid, and thermal considerations, the analysis ensured that the launch latch would meet the necessary performance standards required for safe and effective operation.

The comprehensive evaluation addressed potential risks and failure modes, offering a clear understanding of how the system operates under various conditions. It also provided a foundation for design improvements, ensuring that any identified weaknesses could be mitigated through engineering solutions.

Overall, the analysis confirmed that the launch latch system is capable of performing its intended function with high reliability and minimal risk of failure, laying the groundwork for further testing and validation in the final stages of development.

10 Design Breakdown

All the components of the subassemblies have been designed and assembled to the Launch Latch for fueling liquid rocket engines. The following sections focus on how each subassembly works and will be manufactured for the actual product.

10.1 Assemblies Components

Each subassembly has its own function which is integrated into the full assembly. The subassemblies have been introduced through the analysis and design sections and this section will explicitly describe how each subassembly works and interacts with each other. The subsection 10.1.1 will describe the integrated function of the Launch Latch and each following subsection will describe the different parts of the subassemblies and how the parts interact to perform the desired function.

10.1.1 Final Assembly

The entire assembly is made up of four main assemblies. The structure assembly attaches to the arm assembly, the arm assembly attaches to the actuation assembly, and the arm assembly attaches to the valve assembly. The assemblies work together to create the Launch Latch that can detach the fueling valve remotely followed by moving the fueling valve and other items out of the fuel plume in a timely manner to ensure that no components get destroyed due to the high temperatures. The arm is adjustable to ensure that any angle and height of valve can be connected within the desired height range. A further breakdown of each assembly is discussed next.

Figure 10.1.1. Model of Final Assembly

10.1.2 Structure Components and Assembly

The structure subassembly is the simplest of the assembly when it comes to moving parts. The Structure is made of three main parts and then the feet. There are additional fasteners in the structure that secure the different parts together. The full assembly of the structure can be seen Figure 10.1.2.

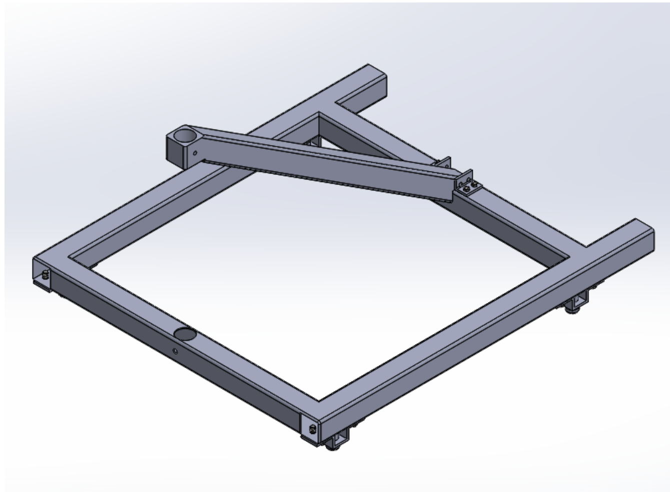

Figure 10.1.2 Full Assembly of the Base.

The base and support are made from mild steel square stock with a width of 2.5 *in* and a thickness of 0.120 *in.* The pole is also made from mild steel, but it is circular tubing with an outer diameter of 2 *in* and a thickness of 0.120 *in*. The bolts and nuts are made from steel. The bracket connecting the base and the support is also made of mild steel.

The different pieces of the structure are all secured with bolts for ease of use. This allows the structure to be put together on site and very portable. The feet are attached to the base by four different bolts per foot support. The bolts are ½ *in* bolts with a length of 1 *in* and fully threaded. These go into a threaded hole in the foot support and base. The foot itself is in a threaded hole which allows the foot to be screwed in or out to adjust the heigh of the stand to ensure levelness. The support is attached to the base by two brackets on the side that are screwed into the base and the support itself. The pole is attached to the support and the base in two separate locations. Both bolts that hold the pole to the structure are 3/8 *in* bolts with a length of 3 *in* and only partially threaded. There is a nut on the back of the bolts to secure it. It is not a lock washer since it needs to be easily detachable. The first one is on the base in the middle of the front steel member. The second one is in the support at the end where the pole goes through it. The pole will hold the rest of the components in the disconnect system. They will be described in the following sections.

10.1.3 Arm Components and Assembly

The primary components of the arm subassembly are the clamps, the arm, and the support bar. These components interact through pinned joints. The arm is pinned to the upper clamp as well as to the support bar about 14 *in* from the base of the arm. The support bar that is pinned to the arm spans to the pinned joint of the lower clamp. The function of the clamps is to attach the arm to the vertical pole via torquing 2 bolts on each clamp. Figure 10.1.3 provides a general layout of the interconnections of these primary components of the subassembly.

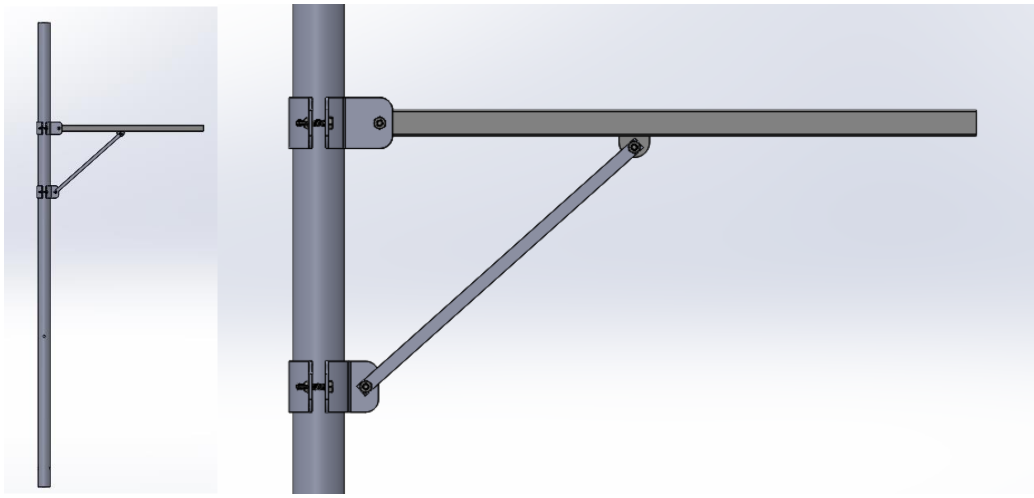

Figure 10.1.3. Reference for the interconnections of the arm subassembly

The arm subassembly in the Launch Latch has two main functions including adjustability and support for the actuation and fluid system, ensuring proper alignment, and a clean connection between the Launch Latch and the rocket's fill port. This adjustability is achieved through three primary motions. Vertical displacement is facilitated by sliding the two circular clamps up or down the pole, allowing precise height adjustments. Rotation about the pole is accomplished by pivoting the circular clamps around the pole's axis, enabling the arm to align the azimuth as needed. Finally, the pitch angle of the arm is controlled by adjusting the distance between the upper and lower clamps. For example, decreasing this distance causes the arm to pitch upward if required. The positions of the clamps, both absolute and relative, drive all these motions. To simplify adjustments and ensure secure torquing of the clamps, wing nuts are installed on each pair of bolts securing the arm. This configuration provides an accessible and effective means of fine-tuning the subassembly for optimal performance.

10.1.4 Actuation Components and Assembly

The actuator subassembly is comprised of two separate parts: the standoff bar and the spring assembly. The standoff bar provides reach when fully extended and supports the valve on one end. The spring assembly provides support and ease of motion to the spring.

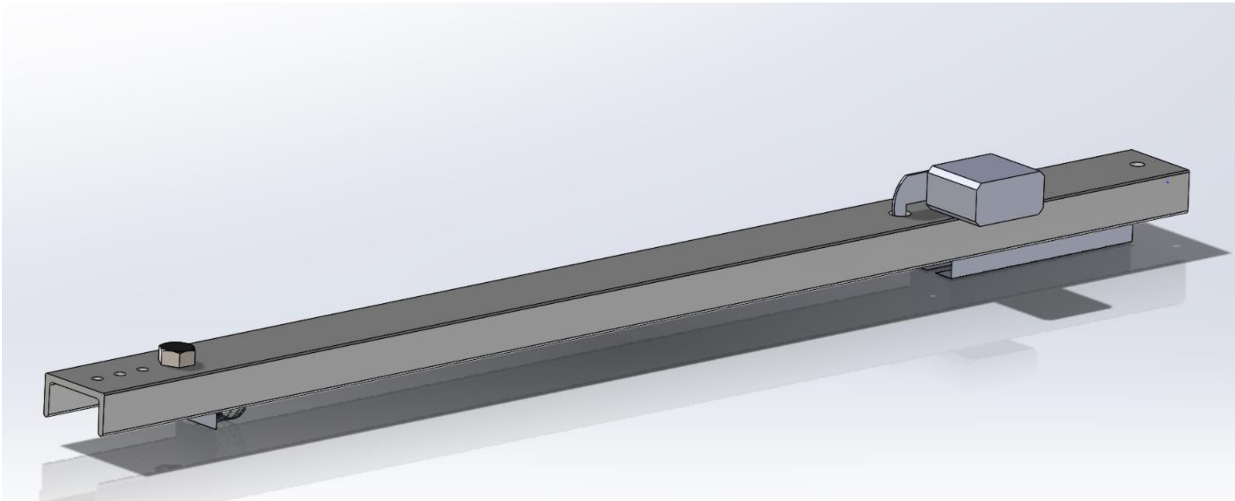

Figure 10.1.4. Full Standoff Bar Assembly

The standoff bar can be seen in Figure 10.1.4. It is made from a C-channel welded to a collar. The collar wraps around the arm and is what slides along the square pipe of the arm. Holes are drilled into the C-channel to facilitate connection to the valve on the rocket-side end, and the spring on the other. Mounted on the top side of the C-channel is the pin, which is controlled via servo. The pin holds the standoff bar in place by being pressed against the arm bar and preventing motion from the spring and can be seen in Figure 10.1.5. On the rocket-side end of the C-channel, there is a stop to prevent shocks to the rest of the structure and damage to the valve. The stop is made of a steel L-bracket bolted into place with a spring secured onto the face. When the bar is actuated, the spring is the first point to make contact with the bar arm, and dampens the impact of the actuation. The spring stop can be seen in Figure 10.1.6.

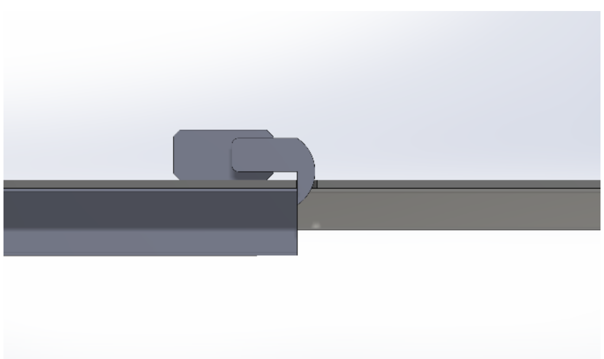

Figure 10.1.5. Pin Catching on Square tubing

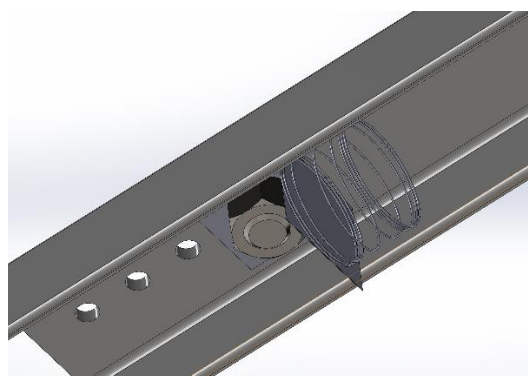

Figure 10.1.6. Stop with Spring

The spring assembly is made to support a constant-force spring. At the base of the arm, there are two small steel plates bolted into the support clamps. These plates extend upwards and support a threaded rod which is bolted into place and holds the spool for the constant-force spring.

10.1.5 Valve Components and Assembly

The valve consists of a male component on the rocket side, and a female component mounted to the retraction arm. Each of these contains a spring-loaded internal plug to prevent fluid flow in the disconnected state. The travel of these plugs is limited by an internal stop, and they are displaced by being forced against each other as the components are fitted together. The male and female components are sealed against each other by means of an O-ring.

To prevent the components from separating in use, a set of balls is housed in holes in the wall of the female component. These holes are tapered towards the bottom to hold the balls captive in the disconnected state. A ridge on the male component displaces the balls during insertion and removal. This travel is constrained by a retention ring that sits around the female component. It is spring loaded in a restrictive position that does not allow the balls to travel, and hence prevents the components from separating.

10.2 Manufacturing considerations and processes

For the production of the Launch Latch, various manufacturing considerations are required to balance manufacturability, cost, and quality of the design. The following subsections will outline the considerations when it comes to the manufacturing process for each subassembly.

10.2.1 Structure Manufacturing Considerations

For the manufacturing process of the structure subassembly, all square tubing will be made from bent metal and welded together to form the square. However, the circular piping will be extruded from a form die to achieve tighter tolerances. The feet support will be cast to ensure it is structurally sound compared to bent sheet metal. All steel stock will be cut to length using a drop saw capable of cutting large cross sections. A drill press will be used to drill holes in the desired locations on the base pieces, support, and pole. A tap will be used for threaded fasteners that do not have a nut attached to the bolt. Once all pieces are cut to length, drilled, and tapped, the base pieces will be welded together to ensure a rigid assembly. The bracket connecting the support and base will be made from L-channel, cut to length with holes for threaded or bolted fasteners.

The assembly process for the structure subassembly can be completed by hand and with an impact driver, as it only requires fasteners: wingnuts for the bolts, which will be hand-tightened, and an impact driver for the bolts connecting the support and base. The simplicity of this assembly makes it ideal for assembly in remote launch locations. The structure is designed to be portable, which is why it is made of multiple pieces.

10.2.2 Arm Manufacturing Considerations

In the manufacturing process of the arm subassembly, all support components—including the arm, support, and vertical pole—are made of steel with hollow cross-sections. These components will be produced via rolling and welding. Additionally, each support member will be drilled in specified locations for fasteners. The 1 *in* square pipe will require further processing including a mounting point for the support bar to be welded as defined in the drawing of the arm. Similarly, the clamps will be rolled to fit the vertical post, then bent to form the flanged sections at each end. Next, hinges are to be welded to the clamps to allow mounting points for the arm and support.

The assembly process for the arm subassembly can be completed by hand as it only requires fasteners which will be hand tighten wingnuts for the clamps and torqued via a wrench for each pinned joint. The simplicity of this assembly is ideal for ease of use while in service.

10.2.3 Actuation Manufacturing Considerations

For the manufacturing process of the actuation subassembly, a 1.25 *in* wide mild steel C-channel will be used for the standoff bar. The collar is made using thick mild steel sheet metal and will be bent into shape using a sheet metal brake. Space must be left on the bottom of the collar such that it can slide around the arm hinges. The collar will be welded to the C-channel. The L-channel for the spring stop is made using the same thick mild steel sheet metal and bent into shape using a sheet metal brake. It will be secured in place with a 3/8 *in* nut and bolt. The spring will be welded to the back face of the stop.

The spring support subassembly will utilize the same thick mild steel sheet metal as standoffs from the arm hinge. The steel sheet will support a 3/8 *in* threaded rod, which will be bolted into place. On the threaded rod, there will be a 3D-printed spool, which holds the constant force spring. The constant force spring will be attached to the standoff bar using a 1/4-20 nut and bolt.

The assembly process for the actuation can be done by hand, as it only requires a wrench to attach the constant force spring to the standoff bar. This makes it ideal for quick construction on the launchpad.

10.2.4 Valve Manufacturing Considerations

The valve assembly will consist of a combination of COTS and machined components. The male and female housing components will be manufactured through a combination of lathe and mill operations. The balls, springs, O-ring, and retention clip will be commercially procured. The internal plugs and their stops will be lathe cut, and the stops will freeze fit into place.

10.2.5 Fluid System Manufacturing Considerations

Since the fluid system (excluding the valve) can and should (for safety reasons) consist of commercially purchased components, a number of part selection considerations can be put under the umbrella of manufacturing considerations.

First and foremost, as specified in Appendix A: Preliminary Design Specifications (PDS), all fluid-containing components must be rated for the pressure and chemical makeup of the intended propellant to be used.

The routing of the fluid system is also important. Any flexible hoses must be properly restrained at certain locations, but not interfere with the required movement of the valve during connection and disconnection. Any rigid tubing should be sufficiently supported so as to not induce stress onto the tube connections.

11 Prototype

For the Launch Latch, the prototype needs to be very close to the actual design that has been detailed in the report because this system will be used by the WiSP club to fuel the liquid rockets that they will be launching. This requires that the scale is one to one to ensure the full range of heights is met. The functionality of the prototype needs to be as close as the design to ensure no failures occur in the field. There were some minor changes when it came to the prototype for manufacturability and cost considerations, but these did not change the functionality of the design. The full prototype design can be seen in Figure 11.1.

Figure 11.1. Full Prototype with a banana for scale

11.1 Prototype Components

The Launch Latch prototype was designed with modularity in mind, allowing for easy portability. This modular approach also enabled simultaneous construction of individual subassemblies, improving efficiency. The prototype's components worked hand in hand to achieve the goals of the disconnect system. The prototype has minor changes when compared to the design of the Launch Latch detailed in the design. Even with the changes, the prototype maintains functionality.

11.1.1 Prototype Workings

The Launch Latch prototype works as the design intended. The structure has adjustable feet that ensure the system remains level on uneven ground. Additionally, the structure and arm are modular which allows for portability. The steel components of the base were cut to length, welded, drilled, and tapped. The structure can be seen in Figure 11.1.1.

Figure 11.1.1. Prototype of the base of the disconnect system with a banana for scale

The arm is adjustable which allows for all angles of valves within the designated height range to be attached. The clamps on the arm that attach to the pole are adjustable via a wrench which allows for ease of access at launch site. The actuation assembly is mounted onto the top of the arm. There is a constant force spring that constantly keeps the sliding bar in tension. This is to ensure when the valve disconnects and the servo is released, the extended bar will be pulled back immediately. The servo has an arm that is preventing the extendable bar from shooting back right away, but once that the servo is engaged the bar slides back. Another spring has been installed to reduce the kinetic energy of the U-channel to ensure the extendable bar does not violently shoot back from the constant force spring. The arm and the actuation system can be seen in Figure 11.1.2.

Figure 11.1.2 Close up of arm (Left) and partially extended state of the bar (Right)

The valve has an actuator that is connected to 120V which then in turns releases the system holding the male and female valves together. Once the actuator is triggered, the coil spring on the actuation spring pulls the extendable bar and valve out of the fuel plume area.

11.1.2 Prototype Differences

There were some minor differences between the prototype and the design. The first small change was that the feet on the base do not have brackets that the feet go into. Instead, the feet are just a threaded screw that goes directly into a threaded hole that were drilled into the base. Also, the are some nuts and bolts that were changed to threaded fasteners in tapped holes. These were located on the support and base where the bracket and support connect. The bracket was also welded to the support instead of fastened.

The arm varied from the true design in two ways, one of which being the clamp thickness, the thicker sheets of metal were found to be difficult to bend to form the rolled and flanged shape of the clamp, so thinner sheet metal was used. The other deviation of the arm can be seen in the left image of Figure 11.1.2, where the prototype uses an L bracket to support the arm instead of the ½ *in* square tube in the design. The use of an L-bracket was used for material availability. This deviation was acceptable because although there was a decrease in moment of inertia compared to a square cross section, the increased thickness provided more than enough margin against buckling.

The actuation method in the prototype varied in that the spring stop was not utilized. Instead, a 3/8 *in* bolt wrapped in foam was used. While this method is crude, it still provides adequate shock damping, is fit for multiple uses, and protects the valve structure from damage. The servo that provides the retraction actuation was not bolted on, but rather in the interest of time was adhesively bonded to the surface of the bar, which had been mechanically sanded to enhance surface adhesion, using a thermoplastic adhesive applied in a molten state to achieve a secure attachment.

Instead of manufacturing the valve from scratch, a commercially available hydraulic quick disconnect was procured. This quick disconnect lacks mounting points for an actuation mechanism or the retraction arm. To compensate, a frame and pull ring were manufactured out of Formlabs rigid resin using stereolithography (SLA) printing as shown in Figure 11.1.3. These parts were fitted to the quick disconnect and solenoid. The release ring of the quick disconnect was modified to accommodate the pull-ring in such a way that force would be transferred in compression against a hard stop, and adhesive was used only to prevent the components from slipping out of place when the solenoid is in the de energized state.

The prototype fluid system was simplified to fit the budget and scope of the prototype. Since the full fluid system cannot be demonstrated within a large blast radius, instead a simple empty gas bottle and plastic tubing that connect from the bottle to the valve demonstrates how the flexible propellant line is able to move with the retraction mechanism (note that this is not pictured in the figures above).

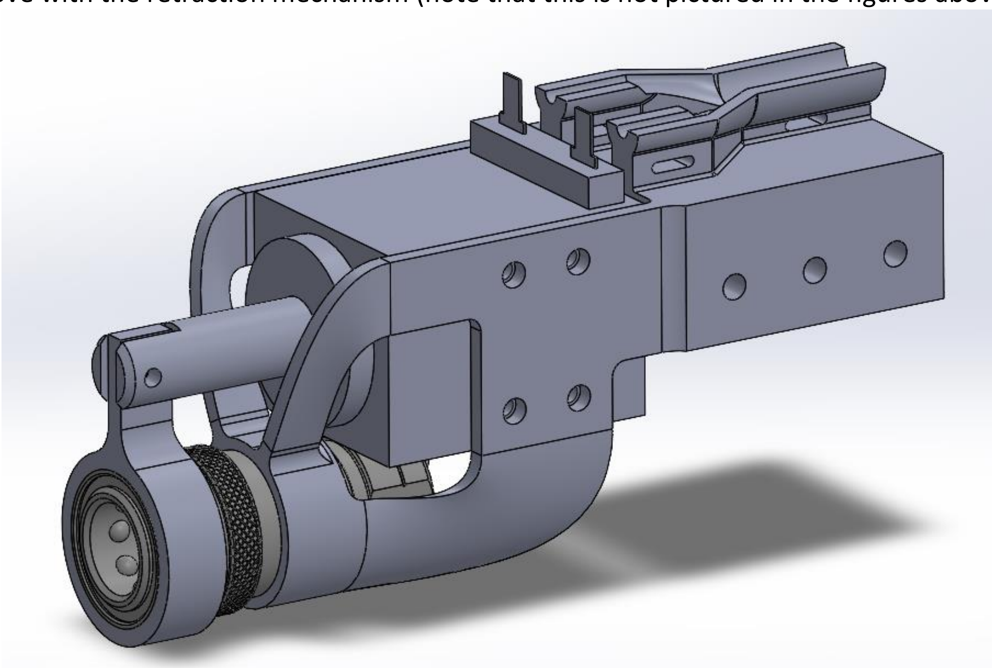

Figure 11.1.3 Prototype Frame and Disconnect Assembly

11.2 Prototype Challenges

One of the key challenges in developing the modular prototype was defining the connections between subassemblies. These connections had to ensure compatibility without interfering with the primary functionality of each section. This was seen in how to mount the valve housing to the actuation assembly without the impact force of the retraction going through the bolts of the solenoid housing of the valve system. Another ill-defined interconnection was of how to mount the tape spring of the U-channel retraction to the fixed structure. This prompted the addition of a spool to be mounted on the arm assembly.

Other challenges that arose with individual parts included the power requirements of valve actuation. The prototype includes a solenoid that requires 120V, which is useful for ensuring sufficient force for valve disconnect in testing, however, it will be unreasonable to supply 120V in the desert for an actual launch.

A challenge that was experienced during production of the arm assembly with the thickness of the clamps. In section 11.1.2, a change from the design was made to use thinner sheet metal than specified in the design. This resulted in a lack of stiffness against the preload of the bolts and resulted in deformation. Additionally, this lack of thickness caused inefficient welds of the hinges due to the variance of thickness between the two parts.

A challenge that was experienced while creating the structure was the size of the steel square tubing and circular tubing. The steel square tubing was 2.5 *in* and the circular tubing was 2 *in.* The square tubing could be decreased by ½ *in* since the added weight was needed to prevent tipping. The large square steel stock was awkward to weld in the MIG welding lab due to the limited space available for welding. Additionally, drilling center holes in a circular tubing was very challenging. The circular tubing was a full 6 *ft* while it was being drilled. The circular tubing had to be drilled on the mill rather than a drill press which took a lot more time than expected. Lastly, for the structure a challenge was the tolerances, the holes already had a built-in tolerance, but that not enough for the bolts to go through in the prototype.

One challenge encountered during integration of the various mechanisms was the mounting of the servo to the bar. Without bolting through the C-channel, it is difficult to mount anything on top since a zip-tie would interfere with the connection point on the angle adjustment linkage. Because of this, thermoplastic adhesive was used instead, and with sufficient reinforcement and surface preparation it resulted in a very strong bond, particularly because the only load transferred by the bond is strictly tangent to the surface of the bar.

12 Conclusion

The Launch Latch project represents a significant milestone in the development of innovative ground support equipment for collegiate and amateur rocketry. By addressing the critical need for a safe, reliable, and adaptable propellant quick-disconnect system, the team demonstrated a comprehensive approach to engineering design, combining structural integrity, operational efficiency, and safety considerations.

This conclusion reflects on how the project met its design objectives, the lessons learned throughout the process, and the opportunities for future advancements. From overcoming challenges during prototyping to validating the system's performance through rigorous analysis, the project has laid a solid foundation for continued innovation in support of rocketry's demanding requirements.

12.1 Design Criteria Evaluation

The Launch Latch design fulfilled all the critical design specifications by combining innovative engineering with robust material selection and thoughtful testing protocols. However, some of the other design criteria in the product design specification were not met. The majority of the criteria laid out in the product design specification were met, and the critical design specifications were met. This is a successful design going off the critical design specifications with room for improvement to satisfy all criteria.

The first critical design specification was that the design needed to be adjustable to various rockets and launch rails. This meant that the design needed to be able to reach fueling ports between 2-6 *ft* and at different angles. The design of the arm is able to attach to the pole from desired range and built in a way to change the angle. The next one is remote operable. The servo and actuator on the valve require electricity and are triggered with a button or a signal. This technically satisfies the remote operability criteria, but it could use some work to increase the range. The plumbing was designed to withstand high pressures that the fuel and oxidizer induce on the system. The valve was designed to be easily mateable and detachable with the flight side connection. This ensures that there are no errors when the valves disconnect. The last critical design specification was that the fluid system and valves are compatible with standard propellent cylinders which were achieved.

The single-pole structure provided ease of alignment, while its lightweight, modular design ensured portability and rapid on-site assembly. The modular structure was adaptable to various rocket sizes and propellant configurations, addressing the requirement for compatibility with different rocket sizes and fluid systems. Because mild steel was used for multiple parts, the disconnect system will rust. Protective coating can be applied to mild steel components to withstand the environmental conditions better in desert launch scenarios, such as high winds and extreme temperatures. The disconnect system will be able to fully function in the desert environment but will not last as many cycles as intended. This is addressed in the maintenance section of the product design specifications because it is supposed to be maintained after each use. This includes cleaning the disconnect system and ensuring no hazardous chemicals remain on it. This will ensure the product lifespan is as stated in the product design specifications.

The product design specifications include the materials and weight of the disconnect system. The weight of the disconnect system was stated to be no more than 200 *lbs* total and no more than 50 *lbs* for each individual item. The overall weight is not close to the 200 *lbs*, however the base of the disconnect is close to the maximum weight. This can be fixed by decreasing the size in another version and including a counterweight. The counterweight would provide the safety the larger steel provides while decreasing the parts weight. This relates to the material as well. The material choice of mild steel was the correct one, but it will need a protective coating to help protect from the environment.

The actuation mechanism, a spring-loaded linear bearing system, achieved rapid and reliable disconnection, protecting sensitive components from exhaust heat and ensuring operational safety. Similarly, the commercial latching valve guaranteed a high-pressure rating and minimized fluid leaks, meeting the performance demands for oxidizer handling. Testing procedures—ranging from leak and pressure tests to functional disconnection simulations—are expected to validate the system's operational integrity due to the commercially sourced valve. The Launch Latch's capability to perform full oxidizer detanking remotely in case of launch aborts addressed critical safety concerns, ensuring compliance with NASA standards and the project's design objectives.

12.2 Lessons learned

The development of the Launch Latch underscored the importance of balancing simplicity, reliability, and performance in engineering solutions. Early design iterations highlighted the challenge of achieving structural stability while maintaining portability. The team learned the value of a focused design approach, such as prioritizing the spring-loaded actuation system for rapid, effective motion rather than more complex alternatives.

Another key lesson was the need for precise alignment mechanisms to accommodate the varied geometries of amateur rocketry systems. The alignment issues encountered during initial tests prompted a redesign of the single-pole structure to allow increased degrees of freedom, improving the system's usability. Before the redesign, there were many challenges that occurred to achieve all design specifications. The initial design required disconnection and reconnection. This simple change would require extreme tolerance and stability of the structure to maintain alignment when disconnect. The initial designs did not come up with a way to reliably reattach to rocket. But after a design consolation with an outside perspective, the question arose of how likely reconnecting would occur. The resulting answer fixed the issues with tolerance and stability while still achieving almost all initial critical design specifications.

It is important to take into account different standards and environmental factors that were not originally consider. The team also gained a deeper understanding of compliance with safety standards and protocols, such as those set by NASA for high-pressure systems. These lessons highlighted the importance of collaboration and adaptability in meeting the multifaceted challenges of engineering projects, particularly those involving dynamic and hazardous conditions. Additionally, the team learned the necessity of accounting for environmental stresses such as UV exposure, abrasion from sand, and thermal cycling throughout the process of designing core mechanisms of each section.

Manufacturing time and processes are key parts to take into account when building a prototype. Manufacturing processes are the easiest to complete when there is a laid-out plan step by step to complete the prototype. There were some occasions while manufacturing the prototype that an egregious error could have been made by doing one step out of order. Welding for the base needed to be done last due to none of the drill presses being able to hold the large base. Fortunately, no errors, occurred in the manufacturing process.

However, once the final assembly was put together there were some obvious errors that did not show in the design or CAD. The first error occurred when the extendable arm was fully extended. The extendable bar and the adjustable bar were pinching under the weight of the valve which prevented the constant force spring engaging. This displayed the importance of prototyping and thinking of the design in actuality to find our potential errors in the design.

12.3 Future Work

While the Launch Latch achieved its initial goals, several avenues for improvement and expansion remain. Future work could explore the integration of aluminum to further reduce the system's overall weight as through analysis the team found significant margins in strength requirements for support members. The base could be weight optimized further by relying on the use of stakes and sandbags to prevent tipping, as both of which will be highly applicable for desert conditions.

The material selection is an area of future work, but that would also consist of a protective coating to help prevent damage from the environment or the exhaust plume. There will be many external factors such has high winds, sand, and hazardous chemicals potentially exposed to the disconnect system. It is important to ensure that any material selected does cause a problem with potential fuel and oxidizers.

The actuation system, while effective, could be optimized for greater energy efficiency and faster response times, potentially through the incorporation of a lower friction sliding surface along with an improved damping system to dissipate the kinetic energy of the retracting U-channel. Alternatively, pneumatic or electronically controlled enhancements could provide this improvement.

As discussed in the challenges of the prototype, the solenoid for the valve retraction will require a redesign to ensure functionality in remote launch locations. However, another future goal includes expanding compatibility to cryogenic propellants would broaden the system's utility for diverse applications in collegiate and amateur rocketry, so a redesign of most fluid components is required. Additionally, enhanced sensor integration, such as pressure or flow rate monitors, could provide real-time feedback to operators, further increasing safety and operational reliability.

Field testing in diverse environmental conditions—such as extreme heat or wind—will help validate the system's versatility and identify areas for further refinement. Lastly, a detailed analysis of cost reduction strategies, including component standardization and manufacturing efficiencies, will ensure the design remains accessible for maintenance.

The insights and advancements realized through future work will not only strengthen the Launch Latch as a product but also contribute to the broader development of safe, efficient, and innovative solutions in amateur and collegiate rocketry.

12.4 Cost

The prototype of the Launch Latch was built at a cost of $500, the prototype demonstrates the primary functionality and modularity of the final design. However, additional investment is required to transition from the prototype to a fully functional system capable of meeting all operational demands and considerations of the future work detailed in section 12.3, including implementing the full fluid system, the simplified version of which was not included in the prototype cost.

This next phase of development requires an additional $800 contract to refine and upgrade the prototype. These funds will support critical advancements such as structural weight reductions, cryogenic fluid components, and improved electronics. By addressing these refinements, the finalized Launch Latch system will deliver operational reliability, adaptability, and safety, supporting the ambitious goals of the WiSP rocketry program and advancing the development of collegiate ground support technology.

12.5 Summary

The Launch Latch project represents a comprehensive effort to address critical needs in collegiate and amateur rocketry ground support systems, emphasizing safety, reliability, and adaptability. By fulfilling the critical design specifications—such as adjustability, remote operability, compatibility with standard propellant systems, and robust performance under high-pressure conditions—the design successfully demonstrated its core functionality. Innovative features like the spring-loaded actuation mechanism, modular structure, and commercial latching valve ensured the system met operational demands while maintaining ease of assembly and portability.

Despite meeting the majority of design criteria, opportunities for refinement remain. Challenges encountered during prototyping and testing highlighted areas for improvement, such as enhancing alignment mechanisms, addressing material durability in harsh environments, and optimizing the actuation system for energy efficiency. Lessons learned from manufacturing and testing underscored the importance of proactive design iteration, compliance with safety standards, and adaptability to environmental factors.

The project laid a strong foundation for future work, with potential advancements including weight reduction, improved material coatings, enhanced compatibility with additional propellants, and integration of real-time monitoring systems. These developments aim to expand the Launch Latch’s capabilities and ensure its long-term reliability and effectiveness. With further investment and refinement, the Launch Latch has the potential to become a pivotal tool in supporting innovative rocketry missions, advancing the field of amateur and collegiate aerospace engineering.

13 References

[1] Bureau of Labor Statistics, "U.S. Bureau of Labor Statistics," U.S. Department of Labor, 29 August 2024. [Online]. Available: https://www.bls.gov/ooh/architecture-and-engineering/aerospace-engineers.htm. [Accessed 24 September 2024].

[2] G. D. Krebs, "Gunter's Space Page," [Online]. Available: https://space.skyrocket.de/doc_chr/lau2023.htm. [Accessed 24 10 2024].

[3] Northrop Grumman, "Space Logistics Services," Northop Grumman, Falls Church, 2020.

[4] Blue Origin, "New Glenn: The Foundation for a New Era," Blue Origin, Kent, 2024.

[5] NASA, "Mobile Launcher Tower Umbilicals and Accessories," NASA, Kennedy Space Center, 2021.

[6] SpaceX, "The Gateway to Mars," SpaceX, Brownsville, 2024.

[7] O. S. U. AIAA, "osuaiaa," AIAA, Oregon State University, 2021. [Online]. Available: https://osuaiaa.com/hale. [Accessed 15 10 2024].

[8] E. Crapo, Director, *Project Design & Build | Auto Disconnect Valve for Hybrid Rocket.* [Film]. Youtube.

[9] T. S. M. Theurich, Director, *Royal Air Force Typhoon GFR4 performing in-flight refueling.* [Film]. U.S. Air Force, 2017.

[10] National Aeronautics and Space Administration, "NASA Standard for Ground-Based Pressure Vessels and Pressurized Systems (PVS)," NASA, Washington, DC, 2022.

[11] NASA, "US 3656781 A: Quick-Disconnect Coupling," United States Patent and Trademark Office, United States, 1972.

[12] Deka Products LP, "US 5116021 A: Quick-disconnect valve," United States Patent and Trademark Office, United States, 1992.

[13] NASA, "US 10730646 B1: Oxidizer nozzle tool and quick disconnect system for fueling," United States Patent and Trademark Office, United States, 2020.

[14] A. Sennott and C. Sharp, "Mojave Sphinx Build, Integration, and Launch Guidebook," Half Cat Rocketry, Orlando, FL, 2024.

[15] M. Taylor, "Improved EN-60529 Dust Chamber for IP5x or IP6x Enclosure Testing," in *2007 IEEE Symposium on Product Compliance Engineering*, Longmont, CO, USA, 2007.

[16] National Aeronautics and Space Administration, "Leak Test Requirements," NASA, Washington, DC, 2023.

[17] Control Products Inc, "What is a Linear Actuator," 2024. [Online]. Available: https://www.cpi-nj.com/what-is-a-linear-actuator/. [Accessed 30 September 2024].

[18] Stober, "Rack and Pinion Servo Geared Motors," 2024. [Online]. Available: https://www.stober.com/products/geared-motors-rack-pinion-drives/#tab-267602. [Accessed 30 September 2024].

[19] GaoXiang, "The Working Principle of Electric Linear Actuator," 24 November 2021. [Online]. Available: https://www.electric-linear-actuators.com/blogs/news-1/the-working-principle-of-electric-linear-actuator. [Accessed 30 September 2024].

[20] Plumbing Supply, "Speedfit Quick Connect Fittings," [Online]. Available: https://www.plumbingsupply.com/push-fit-quick-connect-fittings.html.

[21] Hartford Technologies, "Quick Disconnect Couplings," [Online]. Available: https://hartfordtechnologies.com/precision-balls/ball-applications/quick-disconnect-couplings/.

[22] National Aeronautics and Space Administration, "Standard for the Design and Fabrication of Ground Support Equipment," NASA, Washington, DC, 2013.

[23] The American Society of Mechanical Engineers, "Boiler and Pressure Vessel Code," ASME, New York, NY, 2017.

[24] Asia Industrial Gases Assocation, "Safe Practices for Storage and Handling of Nitrous Oxide," AIGA, Singapore, 2016.

[25] American Society for Testing and Materials, "Standard Specification for Quick Disconnect Couplings (6 in. NPS and Smaller)," ASTM, Conshohocken, PA, 2022.

[26] National Aeronautics and Space Administration, "Requirements for Threaded Fastening Systems in Spaceflight Hardware," NASA, Washington, DC, 2019.

[27] National Aeronautics and Space Administration, "General Welding Requirements for Aerospace Materials," NASA, Washington, DC, 2021.

[28] MetalsDepot, "Round Steel Tube-Welded," MetalsDepot , [Online]. Available: https://www.metalsdepot.com/steel-products/steel-round-tube-welded?gad_source=1&gclid=CjwKCAiAxKy5BhBbEiwAYiW--xLZjMCQHILFSLEFuM_3rbKY3Ep4SvSBuyQTRQ9tNWify1wdXChaqBoC26EQAvD_BwEhttps://www.metalsdepot.com/steel-products/steel-round-tube-welded?gad_source=. [Accessed 2024].

[29] S. F. Hoerner, Fluid-Dynamic Drag, Sighard F. Hoerner, 1965.

[30] M. A. a. H. G. R. B. G. Rabbat, "Friction Coefficient of Steel on Concrete or Grout," *ASCE,* 1985.

[31] Engineers Edge, "Area Moment of Inertia Section Properties Tube/Pipe Calculator," Engineers Edge, 2024. [Online]. Available: https://www.engineersedge.com/calculators/section_square_case_12.htm. [Accessed 2024].

[32] W. J. M. C. E. W. Aaron D Deutschman, Machine Design Theory and Practice, New York: Pearson College Div, 1975.

[33] ASTM International, "ASTM A513/A513M-20, Standard Specification for Electric-Resistance-Welded Carbon and Alloy Steel Mechanical Tubing," West Conshohocken, PA, ASTM International, 2020.

[34] NASA, "Air Properties Definitions," NAVA.gov, 2021.

[35] V. D. d. Silva, Mechanics and Strength of Materials, Portugal: University of Coimbra, 2005.

[36] R. v. Mises, Mechanik der festen Körper im plastisch-deformablen Zustand, vol. vol. 1913, Göttingen: Nachrichten von der Gesellschaft der Wissenschaften zu Göttingen, Mathematisch-Physikalische Klasse, 1913, pp. pp. 582-592.

[37] Barrett, "Fastener Design Manual," NASA Reference Publication, 1990.

[38] ASTM International, Standard Specification for Alloy-Steel and Stainless Steel Bolting for High-Temperature or High-Pressure Service and Other Special Purpose Applications, West Conshohocken, PA: ASTM International, 2023.

[39] S. Gordon and B. J. Mcbride, "Computer program for calculation of complex chemical equilibrium compositions and applications.," NASA, Cleveland, 1994.

[40] C. R. P. Phillip G. Hill, Mechanics and Thermodynamics of Propulsion, Addison-Wesley, 1992.

[41] S. A. K. G. F. Nellis, Introduction to Engineering Heat Transfer, Cambridge University Press, 2020.

[42] The Engineering ToolBox, "Air - Thermophysical Properties," The Engineering ToolBox, 2003. [Online]. Available: https://www.engineeringtoolbox.com/air-properties-d_156.html. [Accessed 7 November 2024].

[43] The Engineering ToolBox, "Friction - Friction Coefficients and Calculator," The Engineering ToolBox, 2004. [Online]. Available: https://www.engineeringtoolbox.com/friction-coefficients-d_778.html. [Accessed 7 November 2024].

[44] W. C. Young, Roark's Formulas for Stress & Strain 6th ed, McGraw-Hill, 1989.

[45] MatWeb LLC, "MatWeb," [Online]. Available: www.matweb.com. [Accessed 07 11 2024].

[46] R. L. Norton, Machine Desingn; An Integrated Approach 3rd ed., Pearson, 2006.

[47] Laird Technologies, "Ceramic Plate Series CP10,31,05 Thermoelectric Modules," [Online]. Available: https://mm.digikey.com/Volume0/opasdata/d220001/medias/docus/5462/CP10_2c31_2c05-SPEC-0209-1590996.pdf?_gl=1*15314uz*_up*MQ..&gclid=Cj0KCQiAoae5BhCNARIsADVLzZf-cGB5i3Pr3EXBqqkz0gc7II6m4ZrzHM9ZXHVa859zhHa9AhfOG7QaAgsTEALw_wcB&gbraid=0AAAAADrbLliF7wko-_hA0b.

[48] NASA, "US 11084710 B1: Refueling tool and quick disconnect," The United States Patent and Trademark Office, United States, 2021.

[49] KegWorks, "Quick Disconnects for 5/16" ID Vinyl Hose," [Online]. Available: https://www.kegworks.com/quick-disconnects-for-5-16-beer-line-and-air-line/.

[50] RobotLab, "Dobot Magician Robotic Arm- Advanced Educational Plan," [Online]. Available: https://www.robotlab.com/store/dobot-robotic-arm. [Accessed 30 September 2024].

[51] Leica Geosystems, "Leica GHT63 Pole Clamp For Field Controller Holder," 2024. [Online]. Available: https://shop.leica-geosystems.com/survey/accessory/geosystems/leica-ght63-pole-clamp-field-controller-holder/buy. [Accessed 24 October 2024].

[52] Software-Factory Schmitz, "Pressure Drop Calculator," 2024. [Online]. Available: https://www.pressure-drop.com/Online-Calculator/.

14 Appendices

14.1 Appendix A: Preliminary Design Specifications (PDS)

Specification	Description	Competition
Performance	- Fills rocket propellant remotely up until launch and pulls back when receiving signal from rocket flight computer. - Fill >5000 cm^3 of desired propellant at flow rate specified by rocket - Dump N_2O in rocket tank into external tank in case of aborted launch. - Plumbing to safely withstand saturated nitrous oxide throughout temperature range of 0°F to 120°F	- Northrop Grumman Mission Extension Vehicle (MEV) - Towers for Orbital Launch Vehicles (OLV) e.g. SLS, Starship, New Glenn - Rocketry Hobbyist/Clubs
Environment	-Should function and be recoverable in a Desert environment (Heat, Dust, Wind, Sun). - Must withstand heat from exhaust and debris kicked up by takeoff - Must withstand: Temp range: 0°F to 120°F ambient Pressure range: 13-17psi Humidity range: 5% to 95% Sand at 30 mph Resting on snow Electronics enclosure rated to IP5X	MEV: Space at GEO OLV and Clubs: Similar to team design, with HLLV subject to stresses and exhaust erosion orders of magnitude more severe.
Maintenance	- Must be maintained after every use - Ensure that no hazardous chemicals remain on surface - Carefully inspect all parts to ensure no structural sections are damaged	MEV: No maintenance possible after launch, reusable/compatible with most GEO satellites. OLV: highly refurbish-able Clubs: reusable with minor adjustments.
Size	- Needs to be portable to different launch sites - When disassembled, needs to fit in a car trunk (roughly size of Chrysler Pacifica or similar minivan)	MEV: Proton-M payload OLV: Large Scale, very few size restrictions. Often permanent installations

	- Adjustable height, must be tall enough to reach fueling point and match angle of valve on rocket (2 ft to 6 ft)	Clubs: Case dependent; depends on transportation requirements
Weight	- Light enough to be carried by two people for a quarter mile (assembly on site an option) - No more than 50 lbs per piece if it is in multiple pieces - Total weight no more than 200 lbs including counterweights	MEV: Proton-M payload OLV: Only structural restrictions Clubs: Similar to our or heavier depending on scale and budget.
Materials	- Plumbing must be compatible with all foreseen fuels, particularly N2O - Tower structure material must be able to withstand high heat & support loads from tank - Materials that will resist corrosion, warping from temperature, and abrasion from sand - Any plastics must be UV safe	Compatibility with fuel and environment of the mission. Sometimes hypergolic, cryogenic, lox, or other propellants that are difficult to handle
Product Life Span	- Reusable for >50 launches, including static fire, test launch, competition launch	MEV: single-use OLV: Program Dependant, 39a in use for >50 years Club: Similar life span as team design
Standards and Specifications	- NASA pressure vessel standards section 4.3-4.4 (link) - NASA disconnect valve specs - IP dust and water ingress rating https://www.iec.ch/ip-ratings	NASA specs NASA Ground Support Standard OLV: propriety standards
Ergonomics and Human Factors	- Remotely operated in conjunction with main rocket ignition signal - Must be easy to adjust and set up on launchpad	All competition includes remote operation
Customer / Market	- Wisconsin Space Program student org. - Other student organizations could use this product to safely disconnect fuel lines for liquid rockets.	OLV: specific to individual program MEV: Satellite owners Club: made specific to the club rocket (same as team design)
Testing	- Component testing before first use, tested for functionality before every subsequent use - Risk assessment will be done once parts are well defined	Every Unit: low production rate with all competitors

	- ASME B31 Pressure Piping Code for pressure and leak tests - Tests: Dry test without rocket to ensure electromechanical function Wet test with low pressure water to ensure plumbing functions Dry test with rocket to ensure coupling and decoupling	
Safety, Public Health, and Human Welfare	- Must have a fail-safe in case of lost connection similar to the existing failsafe on the rocket - The purpose of the product is to isolate the hazards inherent to pressure vessels from the operators - Must have pressure relief valves or burst disks to avoid overpressurization - Must be safe with static electricity, especially with highly flammable fuel - Avoiding and marking pinch points on any moving parts	MEV/OLV: OSHA standards apply to production line. Quick disconnects contribute very minimal safety risk to the overall program. Clubs: same as team design
Economic, Cultural, Social Factors	- This product will neither be marketed at, be made accessible to, or be operated near the general public - This item will allow for more student organizations to fuel liquid rockets safely which will allow more social classes access to aerospace activities - The aerospace industry is rapidly growing in United States and this product would allow more student orgs and hobbyist to grow their knowledge	Quick Disconnect competitors generally are not marketed because designs are specific to a single program.
Environmental Impact	- Most material to be scrapped after lifespan. - Minimize leakage to help the environment. Will prevent additional hazardous gasses from entering the environment. - Structural components out of recyclable metals - There are metals that come from the ground most likely involved in the design which does not help with the environment or global warming.	MEV: could contribute to space trash. Eventually burns up in atmosphere. Orbital Launch Vehicles/Clubs: most of the design is recyclable metals. No positive effects on the environment

14.2 Appendix B: EES Thermodynamic Analysis

File:I:\EMA469\ees.EES 11/4/2024 9:58:55 PM Page 1
EES Ver. 11.907: #100: For use only by Students and Faculty, College of Engineering University of Wisconsin - Madison

```
"Define initial conditions and parameters"
V_source = 13.4 [L]*Convert(L,m^3)            "Volume of source tank"
V_rocket = 3.6 [L]*Convert(L,m^3)             "Volume of rocket tank"
T_rocket[1] = 25 [C]                          "Initial temperature in rocket tank (room temperature)"
T_source[1] = 25 [C]                          "Initial temperature in source tank (room temperature)"
delta_T = 10 [C]                              "Initial guess for temperature drop in source tank"
percent = 0.75 [-]                            "Target percentage of N2O to transfer"

"Initial Quality and Pressure Calculations"
x_rocket[1] = 0.0                             "Assume rocket tank is initially fully liquid"
x_source[1] = 0.0                             "Assume source tank is initially fully liquid"

"Calculate initial properties in the rocket tank at initial temperature"
P_rocket[1] = Pressure(NitrousOxide, T=T_rocket[1], x=x_rocket[1])  "Pressure in rocket tank (assume fully liquid)"
rho_rocket[1] = Density(NitrousOxide, T=T_rocket[1], x=x_rocket[1]) "Density of N2O in rocket tank at T_rocket[1]"
m_rocket[1] = V_rocket * rho_rocket[1]        "Initial mass of N2O in rocket tank"
m_transfer = percent * m_rocket[1]            "Target mass to transfer (% of initial rocket tank mass)"

"Calculate initial properties in the source tank at initial temperature"
P_source[1] = Pressure(NitrousOxide, T=T_source[1], x=x_source[1])  "Pressure in source tank (assume fully liquid)"
rho_source[1] = Density(NitrousOxide, T=T_source[1], x=x_source[1]) "Density of N2O in source tank at T_source[1]"
m_source[1] = V_source * rho_source[1]        "Initial mass of N2O in source tank"

"Define temperature in source tank after cooling and calculate new properties"
T_source[2] = T_source[1] - delta_T           "Temperature of source tank after cooling"
P_source[2] = P_sat(NitrousOxide, T=T_source[2])     "Saturation pressure of N2O in source tank at T_source[2]"
rho_source[2] = Density(NitrousOxide, T=T_source[2], x=0) "Assume fully liquid after cooling, adjust x if needed"
m_source[2] = m_source[1] + m_transfer        "New mass in source tank after transfer"

"Calculate quality in the source tank after transfer and cooling"
x_source[2] = Quality(NitrousOxide, v=1/rho_source[2], T=T_source[2])  "Calculate quality based on P and T in source tank"

"Calculate updated mass and quality in rocket tank after transfer, keeping rocket tank temperature constant"
T_rocket[2] = T_rocket[1]                     "Assume rocket tank remains at T_rocket[1] (constant temp)"
P_rocket[2] = P_rocket[1]                     "Pressure in rocket tank remains the same if temperature is constant"
m_rocket[2] = m_rocket[1] - m_transfer        "Remaining mass in rocket tank after transfer"
x_rocket[2] = Quality(NitrousOxide, v=V_rocket/m_rocket[2], T=T_rocket[2])  "Calculate quality in rocket tank based on
conditions"

"Calculate pressure differential and check if it meets the required threshold"
dP = P_rocket[1] - P_source[2]                "Resulting pressure difference to drive transfer"
dP_req = 0.20 * P_rocket[1]                   "5% of initial rocket tank pressure as required differential"
```

SOLUTION

Unit Settings: SI C kPa kJ mass deg

δ_T = 10 [C] dP = 1147 [kPa] {166.4 [psi]} dP_{req} = 1130 [kPa] {163.9 [psi]}

$m_{transfer}$ = 2.006 [kg] percent = 0.75 [-] V_{rocket} = 0.0036 [m^3]

V_{source} = 0.0134 [m^3]

No unit problems were detected.

Arrays Table: Main

	$m_{source,i}$ [kg]	$P_{rocket,i}$ [kPa]	$P_{source,i}$ [kPa]	$T_{rocket,i}$ [C]	$T_{source,i}$ [C]	$m_{rocket,i}$ [kg]	$\rho_{rocket,i}$ [kg/m³]	$\rho_{source,i}$ [kg/m³]	$x_{rocket,i}$ [-]
1	9.955	5651	5651	25	25	2.675	742.9	742.9	0
2	11.96	5651	4504	25	15	0.6686		820.7	100

14.3 Appendix C: Arm and Joint MATLAB Calculations

```
% Units (in, s, lb, degree F) unless otherwise specified

% Inputs
pitch = 0; % pitch angle of arm
    % Square pipe
        lbar = 24; % Length of square pipe
        sbar = 1; % side length of square pipe
        tbar = 0.065; % Wall thickness of square pipe

    % Support bar
        lsup = 10*sqrt(2); % length of support bar

        dsup = 10; % distance from bar hinge to support hinge
        hsup = 3; % distance from support reaction and x direction

    % actuation/external factors
        Wact = 7; % weight of actuation
        dact = lbar + 20; % distance to COM of actuation
        hdis = 0; % height of disconnect force
        Wclamp = 2; % weight of clamp
        Wpipe = 3; % weight of piping
        dpipe = 30; % distance to COM of piping

    % pins/bolts
        diapin = 1/4; % diameter of double shear pin
        diaboltup = 1/4; % diamter of bolts on upper clamp
        diaboltdown = 1/4; % diamter of bolts on lower clamp
        diapinsup = 1/4; % diamter of bolts on lower clamp

% Constants
rhom = 0.284; % density of steel
rhoa = 1.225 ; % density of air [kg/m^3]
pn2o = 1100; % pressure of N2O
Tamb = 120; % ambient temperature
Cdsquare = 2.05; % drag coefficient for flow over a square pipe
Cdsup = 1.17; % drag coefficient for flow over perp plate
V_inf = 8.9408*1.5; % speed of wind [m/s]
E = 29e6; % elastic modulus of steel
axyield = 32000; % axial yield stress for steel
shearyield = axyield/sqrt(3); % yield for steel in shear

% Geometries from known
pitchrad = deg2rad(pitch);
Anoz = pi * (1/8)^2; % area of nozzle
sbarin = sbar - 2*tbar; % inner length of square tube
Vbar = lbar * ((sbar)^2 - (sbarin)^2); % Volume of bar
posttheta = pi/2 + pitchrad; % angle between post and arm
theta3 = asin(dsup*sin(posttheta)/lsup);
thetasup = pi - theta3 - posttheta;
dclamp = lsup * sin(thetasup)/sin(posttheta); % distance between clamps
Ibar = (sbar^4 - sbarin^4)/12; % moment of inertia of the square tube
```

```
% Forces
Wbar = rhom * Vbar; % weight of bar

misuse = 20; % load due to misuse

% BAR FBD
Rsup = (Wact*dact + Wbar*(lbar/2) + misuse*lbar) / (cos(thetasup)*hsup +
sin(thetasup)*dsup);
Rxbar = -Rsup*cos(thetasup);
Rybar = Wbar+Wact-Rsup*sin(thetasup)+misuse;
```

Support Optimization

minimize weight while being above the buckling line

```
ssupguess = linspace(0.1,1,100); % potential support widths
wallsupguess = linspace(0.001,0.02,100); % potential support wall thicknesses
[W,T] = meshgrid(ssupguess,wallsupguess);

Asup = W.^2 - (W-2.*T).^2; % cross sectional area of the support bar
Isup = ((W.^4) - (W-2.*T).^4)./12; % moment of inertia of the support bar

% support yield / buckling
% rgyro = sqrt(Isup./Asup);
% slendrat = lsup./rgyro;

kbuck = 1;
Pcrit_b = (pi^2*E.*Isup)./(kbuck*lsup).^2;
SFsupbuck = Pcrit_b./Rsup;

sigsup = Rsup./(Asup); % axial stress in support
SFsupcomp = axyield./sigsup;

[C, h] = contour(W, T, SFsupbuck,[3,3]); % only plot where SFsupbuck = 3
set(h, 'EdgeColor', 'red'); % Set the color to red
clabel(C, h, 3); % label the contour line
xlabel('Support Width (in)');
ylabel('Support Wall Thickness (in)');
hold on
[C, h] = contour(W, T, SFsupcomp,[2,2]); % only plot where SFsupcomp = 2
set(h, 'EdgeColor', 'blue'); % Set the color to red
clabel(C, h, 2); % label the contour line
hold off
legend('Buckling','Axial Yielding')

ssup = 0.5;
wallsupmin = min(T(SFsupcomp(:,45) >= 2, 45));
wallsup = 0.049;
```

Support FBD

```
Wsup = rhom * lsup* (ssup^2-(ssup-2*wallsup)^2);
Rxsup = Rsup*cos(thetasup);
Rysup = Wsup + Rsup*sin(thetasup);

% Double shear pin at clamp
Rbarshear = sqrt(Rxbar^2+Rybar^2);
taudshear = (4/3)*Rbarshear/(2*(pi * diapin^2/4));

% Single shear pin at clamp
Rclampdown = sqrt(Rxsup^2 + Rysup^2);
tausshear = (4/3)*Rclampdown/(pi*diapinsup^2/4);

% Single shear pin at bar and support
taushearsup = Rsup/(pi*diapinsup^2/4);

% FBD of upper clamp
Ffup = Wclamp - Rybar;
    % Clamping force needed
    K = 0.3; % Nut factor
    mus = 0.74; % static friction factor of clamp on post
    Tboltup = K * (Ffup/mus)*diaboltup;

% FBD of lower clamp with clamping force
Ffdown = Wclamp - Rysup;
    % Clamping force needed


     Tboltdown = K * (Ffdown/mus)*diaboltdown;

 % bearing stress
     % upper clamp
     metalt = 1/8; % thickness of bearing support
     Abarbear = metalt * (diapin *sin(pi/3)); % projected area of when 1/3 of
 bolt is in contact
     sigbear = (Rbarshear/2)/Abarbear;
     SFbearA = axyield/sigbear;

     % support/bar reaction
     sigbearsup = Rsup/Abarbear;
     SFbearB = axyield/sigbearsup;

     % lower clamp
     sigbearlower = Rclampdown/Abarbear;
     SFbearC = axyield/sigbearlower;

 SFdshear = shearyield/taudshear;
 SFsshear = shearyield/tausshear;
 SFshearsup = shearyield/taushearsup;

 % Prints
 Wtotal = Wbar + Wact + Wsup + 2*Wclamp;
 CG = Wbar*(lbar/2)/Wtotal + Wsup/Wtotal * (lsup*cos(thetasup)/2)+ Wact/
 Wtotal * (dact) + Wclamp*2/Wtotal * (3) ;


 % square tube bending
 Mbar = Wbar*((lbar-dsup)/lbar) * ((lbar-dsup)/2) + misuse*(lbar-dsup)
 +Wact*(dact-dsup);
 sigbend = Mbar * (sbar/2)/Ibar;
 SFbend = axyield/sigbend;
```

Published with MATLAB® R2024b

14.4 Appendix D: Structure Matlab Analysis Code

```
% Analysis
clc;
clear;

% Counter Weight
%w = linspace(1,150,150);
h = (75.5); %in Worst case scenario for tipping

% Weight
Wft = 3.90; %lbs/ft
wb = (2*31+2*42)/12*Wft; %lbs base
ws = (39.81+2.5)/12*Wft; %lbs support
wp = 75.5/12*2.94; %lbs pole
wf = 4*2; %lbs All feet
wtot = wb+ws+wp+wf;

% Parts Center of Mass (from back left as origin)
xb_com =
((2*21*42/12*Wft)+40.75*(35/12*Wft)+7.25*(35/12*Wft))/(Wft*(42/12+35/12+35/12)); %in
yb_com = 3.75; %in
zb_com = 18; %in

xs_com = ((16.75+6)*(39.81/12*Wft)+40.75*(2.5/12*Wft))/(Wft/12*(39.81+2.5));
ys_com = ((15.75)*(39.81/12*Wft)+25.25*(2.5/12*Wft))/(Wft/12*(39.81+2.5));
zs_com = 18; %in

xp_com = 40.75;   xf_com = (4*9+4*39)/8; %in
yp_com = 38.5;    yf_com = 2; %in
zp_com = 18;      zf_com = 18; %in

% System Center of Mass
x_com = (xf_com*wf+wb*xb_com+ws*xs_com+wp*xp_com)/(ws+wp+wb+wf);
y_com = (yf_com*wf+wb*yb_com+ws*ys_com+wp*yp_com)/(ws+wp+wb+wf);
z_com = (zf_com*wf+wb*zb_com+ws*zs_com+wp*zp_com)/(ws+wp+wb+wf);

% Forces
Fx1 = 47.83; %lbs
Fy1 = 35.46; %lbs
Fz1 = 0.7; %lbs
Fx2 = -47.83; %lbs
Fy2 = -48.13; %lbs
Fz2 = 0.08; %lbs
mu = 0.57; %Friction Coeffiecent for Steel against dry concrete
% Ff = -1/2*mu*(ws+wp+wb+wf+w+Fy1+Fy2); %lbs
% N = 1/2*(ws+wp+wb+wf+w+Fy1+Fy2); %lbs

V = 44; %ft/s
rho = 2.327*10^(-3); %slugs/ft^3
C_dp = 1.2; %Drag coefficent for pole
C_dr = 2; %Drag Coefficent for rectangle stock
```

```
p_p = 1/2*rho*V^2*C_dp*75.5*pi*0.00694444;
p_rx = 1/2*rho*V^2*C_dr*21.5*2.5*0.00694444;
p_rz = 1/2*rho*V^2*C_dr*39.8*2.5*0.00694444;

% Sum of Forces and Moments About Front Edge
syms w
eq2 = 0 == Fy1+Fy2-(ws+wp+wb+wf)-w;
eq6 = w*(36)+Fx1*(75.5+1.75)+Fx2*(75.5+1.75-6)+Fy1*(5)+Fy2*(5)-p_p*(75.5/2-
1.75)+wtot*(40-x_com) == 0;
values = vpasolve(eq6,w,-5)


cw = linspace(-25,25,150);
for i=1:length(cw)
    N(i) = -1/2*(Fy1+Fy2-(ws+wp+wb+wf)-cw(i));
    M(i) = cw(i).*(36)+Fx1*(75.5+1.75)+Fx2*(75.5+1.75-6)+Fy1*(5)+Fy2*(5)+wtot*(40-
x_com)-p_p*(75.5/2-1.75);
end

figure;
plot(cw,M)
xlim([-25 25])
xlabel('counterweight (lbs)')
ylabel('Moment (in-lbs)')
title("Tipping Moment vs Counterweight")

% Full Pole
Rx = -p_p-Fx1-Fx2
Ry = wp-Fy1-Fy2
Mz = p_p*h/2+Fz2*(h-6)+Fz1*h

I = pi/64*(2^4-(2-.140)^4);
sigma_bending = Mz*(1)/I

% Internal Cut
c = 26.5
RxI = -p_p-Fx1-Fx2
RyI = wp*(h-c)/h-Fy1-Fy2
MzI = p_p*(h/2-c)+Fz2*(h-6-c)+Fz1*(h-c)

sigma_bendingI = MzI*(1)/I

% Feet Analysis
D = .75;
h1 = .08333;
TPI = 6;

D_p = D-h1;
load = ((-wtot+Fy1+Fy2));
d_m = D/2-h1/2;
d_o = D-2*h1;
```

```
n = TPI/2;
p = 1/TPI;
b = 1/2*p;

sigma_bearing = load/(pi*d_m*h1*n)
shear = 3*load/(2*pi*d_o*n*b)
sigma_c = load/(pi/4*((D+D_p)/2)^2)
max_shear = sqrt((sigma_c/2)^2+shear^2)
```